96.15

Reprinted from JOURNAL OF THE ATMOSPHERIC SCIENCES, Vol. 48, No. 5, 1 March 1991
American Meteorological Society

Determination of the Optical Thickness and Effective Particle Radius of Clouds from Reflected Solar Radiation Measurements. Part II: Marine Stratocumulus Observations

TERUYUKI NAKAJIMA, MICHAEL D. KING AND JAMES D. SPINHIRNE

LAWRENCE F. RADKE

Determination of the Optical Thickness and Effective Particle Radius of Clouds from Reflected Solar Radiation Measurements. Part II: Marine Stratocumulus Observations

TERUYUKI NAKAJIMA,* MICHAEL D. KING AND JAMES D. SPINHIRNE

Laboratory for Atmospheres, NASA Goddard Space Flight Center, Greenbelt, Maryland

LAWRENCE F. RADKE**

Department of Atmospheric Sciences, University of Washington, Seattle, Washington

(Manuscript received 19 March 1990, in final form 19 September 1990)

ABSTRACT

A multispectral scanning radiometer has been used to obtain measurements of the reflection function of marine stratocumulus clouds at 0.75, 1.65 and 2.16 μm. These observations were obtained from the NASA ER-2 aircraft as part of the First ISCCP [International Satellite Cloud Climatology Project] Regional Experiment (FIRE), conducted off the coast of southern California during July 1987. Multispectral images of the reflection function were used to derived the optical thickness and effective particle radius of stratiform cloud layers on four days. In addition to the radiation measurements, in situ microphysical measurements were obtained from the University of Washington Convair C-131A aircraft. In this paper we compare remote sensing results with in situ observations, which show a good spatial correlation for both optical thickness and effective radius. These comparisons further show systematic differences between remote sensing and in situ values, with a tendency for remote sensing to overestimate the effective radius by $\sim$2–3 μm, independent of particle radius. The optical thickness, in contrast, is somewhat overestimated for small optical thicknesses and underestimated for large optical thicknesses. An introduction of enhanced gaseous absorption at a wavelength of 2.16 μm successfully explains some of these observed discrepancies.

Marginal probability density functions of optical thickness, liquid water path and effective radius have been derived from our remote sensing results. The joint probability density function of liquid water path and effective radius shows that the effective radius increases as the liquid water path increases for optically thin clouds, in contrast to optically thick clouds for which the effective radius decreases with increasing liquid water path.

1. Introduction

Marine stratocumulus clouds over dark ocean surfaces are known to modulate the radiation budget of the ocean–atmosphere system through their large areal extent, temporal persistence and high reflectively to solar radiation. Moreover, these planetary boundary layer (PBL) clouds of the marine subtropics affect climate through coupling of radiative, microphysical and convective processes having largely different time scales (Betts and Ridgway 1989). In spite of their importance, however, general circulation models (GCMs) have serious deficiencies in their simulation of PBL clouds, due in large part to their inability to represent the effects of subgrid-scale fractional cloudiness (Randall et al. 1985). This inability to adequately simulate the formation, maintenance and dissipation of stratocumulus cloudiness was one of the major motivations for the marine stratocumulus intensive field observation (IFO) component of the First ISCCP Regional Experiment (FIRE; Albrecht et al. 1988), itself an element of the International Satellite Cloud Climatology Project (ISCCP; Schiffer and Rossow 1983). The IFO provided high spatial and temporal resolution data of marine stratocumulus clouds for the purpose of validating methods for inferring the optical and microphysical properties of stratiform cloud layers, including ISCCP algorithms for retrieving cloud properties.

For the purpose of validating remote sensing techniques, marine stratocumulus clouds have many advantages. These horizontally extensive clouds are quite uniform and overlie a dark ocean surface, thereby reducing problems associated with the radiative properties of finite clouds and of surface reflection. Furthermore, their high temperature ensures that these clouds are composed of liquid water droplets for which Mie scattering by spherical particles is applicable. Finally, the relatively low concentration of anthropogenic graphitic carbon particles assures that these clouds may be treated as pure water clouds with little excess ab-

* Permanent affiliation: Research Center for Atmospheric and Oceanic Variations, Faculty of Science, Tohoku University, Sendai 980, Japan.

** Current affiliation: National Center for Atmospheric Research.

Corresponding author address: Dr. Michael D. King, NASA/Goddard Space Flight Center, Code 913, Greenbelt, MD 20771.

sorption due to impurities (Twohy et al. 1989; King et al. 1990). These conditions permit us to study the well known but still unresolved problem of anomalous absorption by clouds (Stephens and Tsay 1990). Our ability to retrieve cloud droplet size is also important because recent studies have shown that these clouds are easily modified by aerosol emissions from ships (Radke et al. 1989) and by anthropogenic cloud condensation nuclei (CCN) emissions from cities such as San Francisco (Durkee 1989). Such modifications of cloud microphysical properties may further lead to changes in fractional cloudiness and hence climate (Albrecht 1989).

In the first paper of this study (Nakajima and King 1990, hereafter referred to as Part I) we described an efficient algorithm for simultaneously determining the optical thickness and effective particle radius of clouds from multispectral reflected solar radiation measurements. In addition to algorithm development studies, we emphasized the need for aircraft validation experiments to assess the validity and accuracy of such remote sensing methods. In the present paper we present results from an analysis of measurements obtained during four days of FIRE marine stratocumulus observations conducted off the coast of San Diego, California during July 1987. Among the many outstanding features of the IFO dataset is the fact that remote sensing measurements are available from multiple aircraft and satellite platforms, and that these observations were often coordinated with aircraft in situ microphysical measurements.

The intent of this paper is to provide comparisons of remote sensing and in situ estimates of cloud optical and microphysical properties. The remote sensing measurements were obtained using the 0.75, 1.65 and 2.16 μm channels of the Multispectral Cloud Radiometer (MCR) described by Curran et al. (1981) and King (1987), which was flown on the NASA ER-2 aircraft during FIRE. The remote sensing-derived cloud optical thickness and effective radius thus derived will then be compared to comparable values inferred from nearly simultaneous in situ microphysical measurements obtained from the University of Washington Convair C-131A aircraft. Such comparisons are especially important since similar analyses by Twomey and Cocks (1989) and Rawlins and Foot (1990) have shown that cloud droplet radii inferred by remote sensing often exceed those obtained from in situ microphysical measurements. The latter study is particularly relevant, since their data were obtained during FIRE using a different radiometer and analyzed using a different technique than ours.

2. Summary of observations

Comprehensive measurements of marine stratocumulus clouds were acquired off the coast of southern California from 29 June–18 July 1987 as part of the FIRE IFO program. This extensive set of field experiments was designed to take advantage of sophisticated remote sensing and in situ instrumentation onboard aircraft, satellites, tethered balloons and on the surface of San Nicolas Island (Albrecht et al. 1988). During this period, large areas of the eastern Pacific were covered by stratocumulus clouds as a result of subsiding warm air aloft, together with a strong high pressure system over the cold oceanic surface (Kloesel et al. 1988). Figure 1 illustrates a GOES-6 visible image of marine stratocumulus clouds obtained at 1715 UTC (1015 PDT) on 10 July, upon which is superimposed the location and direction of flight of the NASA ER-2 high altitude aircraft. Since the center of the high pressure system was typically located in the vicinity of 35°N, 140°W, boundary layer winds blew from a northerly direction, resulting in a cloud pattern oriented along the wind direction. The cloud deck on this day was optically thick and quite uniform, especially the portion overflown by the ER-2 aircraft during flight line 4 (0939–0951 PDT). This stratocumulus cloud layer was studied in detail by both the ER-2 and the University of Washington C-131A boundary layer aircraft on this day (cf. King et al. 1990). The bright line of clouds oriented between 33.8°N, 121.3°W and 32.4°N, 120.8°W is the cloud layer modified by ship track effluents that was penetrated by the C-131A aircraft at 0856–0909 PDT (Radke et al. 1989).

a. Aircraft and satellite measurements

Table 1 summarizes the times and locations of all flight legs used in this study. These include aircraft measurement on four days (7, 10, 13 and 16 July) and Landsat-5 satellite measurements on two days (7 and 16 July). The ER-2 aircraft, which flew at a nominal altitude of 18 km, was equipped with a cloud and aerosol lidar system (Spinhirne et al. 1989), upward- and downward-looking seven-channel narrowband solar flux radiometers, and spectral scanning radiometers. The C-131A aircraft flew primarily within the clouds to obtain in situ measurements of cloud microphysics and solar radiation.

On 7, 10, and 13 July the ER-2 and C-131A were tightly coordinated in space and time. In the analyses to be presented below, we typically made use of two consecutive flight legs of the C-131A over nearly the same location: 1) a level flight leg for measuring the horizontal distribution of cloud microphysics near the geometric center of the cloud, coordinated where possible with the ER-2 aircraft, and 2) a vertical ascent or descent for measuring the vertical distribution of cloud microphysics as well as the location of the cloud base and cloud top altitudes. Since the nominal aircraft speed of the ER-2 (200 m s^{-1}) greatly exceeds that of the C-131A (80 m s^{-1}), time differences of up to 50 min occurred between aircraft at a fixed location. On 13 July two vertical profiles were obtained from the C-

TABLE 1. Summary of measurements obtained during the FIRE marine stratocumulus IFO that are used in the analyses presented in this study. The latitude, longitude and time of the start and end of each flight line are given for the NASA ER-2 and University of Washington C-131A aircraft and for the Landsat-5 satellite.

Date	Platform	Flight leg (°N, °W) Start	End	Time (PDT)	Comment
7 July	C-131A	31.72, 122.18	31.15, 121.93	1139–1151	Level
	C-131A	31.95, 121.17	31.55, 122.14	1039–1101	Profile
	ER-2	31.08, 121.91	31.97, 122.26	1101–1110	
	Landsat-5	31.01, 122.45	32.52, 122.15	1107	
10 July	C-131A	31.84, 121.37	31.22, 120.10	0922–0951	Level
	C-131A	31.58, 120.80	31.64, 120.93	1012–1017	Profile
	ER-2	31.86, 121.40	31.20, 120.08	0939–0951	
13 July	C-131A	31.77, 120.48	31.71, 120.58	1057–1100	Level-east
	C-131A	31.81, 120.36	31.70, 120.62	1055–1101	Profile-east
	C-131A	31.55, 120.94	31.46, 121.13	1108–1112	Level-west
	C-131A	31.59, 120.89	31.44, 121.16	1106–1113	Profile-west
	ER-2	32.06, 119.87	31.34, 121.40	1048–1101	
16 July	C-131A	31.48, 121.09	31.91, 120.17	1033–1054	Level
	C-131A	31.57, 120.88	31.39, 121.24	1117–1126	Profile
	ER-2	32.07, 120.94	30.82, 121.21	1053–1105	
	Landsat-5	31.01, 120.91	32.52, 120.61	1100	

131A, with only brief (~3–4 min, 15–20 km) sections of level flight in the center of the clouds during the profile periods. As a consequence, the data for the horizontal distribution of cloud microphysics is short compared to corresponding MCR data on this day. On 7 and 16 July flight legs of the ER-2 and C-131A were coordinated with overpasses of the Landsat-5 satellite, which occurred around 1100 PDT. The purpose here was to compare aircraft radiation measurements with comparable observations obtained with the Thematic Mapper (TM) onboard the satellite, as well as to determine in situ cloud microphysical information from the boundary layer aircraft.

b. *Cloud microphysics measurements*

The University of Washington C-131A research aircraft was well instrumented for monitoring cloud microphysics, cloud radiative properties and the characteristics of aerosols interstitial to and within the cloud droplets. The primary instruments of interest to the present investigation of water clouds are: 1) a Johnson-Williams hot wire probe for measuring the cloud liquid water content, mounted in a pylon on the fuselage near the nose of the aircraft, and 2) three Particle Measuring Systems Inc. (PMS) cloud physics probes for measuring the cloud droplet size distribution between 1.4 and 2250 μm in radius. This was accomplished using an FSSP-100, an OAP-200X cloud probe and an OAP-200Y precipitation probe. The FSSP was mounted well below the fuselage of the aircraft and well in front of the propellor arc, and was thus considered to be in nearly free-stream air unaffected by the aircraft. The OAP probes were mounted under the left wing about midway between the wing tip and engine nacelle, thereby avoiding the serious wing tip vortex distortions forecast by King (1984) and described by MacPherson and Baumgardner (1988).

Calibration was confirmed on the FSSP and OAP probes by injection at flight speeds of spherical glass beads of known size. During FIRE the FSSP experienced some optical deterioration and performance losses which were corrected to the maximum extent possible by objective analysis after the experiment. Because of the comparatively low droplet concentrations found in marine stratus clouds, we did not apply coincidence or dead-time corrections to the FSSP data as suggested by Baumgardner et al. (1985) and Brenguier (1989). A more complete description of these instruments can be found in Knollenberg (1981).

c. *Radiation measurements*

The NASA ER-2 aircraft was equipped with the Multispectral Cloud Radiometer (MCR), a seven-channel cross-track scanning radiometer designed to measure the reflected (six channels) and emitted (10.8 μm) radiation with an instantaneous field of view of 7 mrad in a swath ±45° of nadir. This instrument, described in detail by Curran et al. (1981) and King (1987), was mounted in the back portion of the left-wing superpod of the aircraft. For the marine stratocumulus clouds that we observed during FIRE, which typically had cloud tops near 1 km, the spatial resolution of the radiometer was approximately 120 m at nadir.

Radiometric calibration of the six near-infrared channels of the MCR was obtained by observing the output of a 183 cm integrating sphere maintained at Goddard Space Flight Center. The sphere is coated with 12–14 coats of a highly reflecting $BaSO_4$ paint and internally illuminated by a series of up to 12 quartz-halo-

gen lamps. The MCR was calibrated one month prior to the FIRE marine stratocumulus IFO by viewing a 45° plane mirror placed in front of the 25 cm entrance aperture on the side of the sphere.

In addition to the microphysical instrumentation described above, the C-131A aircraft contained a multiwavelength Cloud Absorption Radiometer (CAR) for measuring the angular distribution of scattered radiation from zenith to nadir at 13 wavelengths between 0.50 and 2.29 μm (King et al. 1986). This instrument, mounted in the nose of the aircraft, was calibrated at Goddard by viewing the output of a 122 cm integrating hemisphere in addition to the integrating sphere. The magnitude of the intensity incident on the radiometer was varied both by changing the number of lamps illuminating the integration sources as well as by introducing neutral density filters in the path of the radiation.

On 13 July 1987 the C-131A and ER-2 flew a tightly coordinated mission consisting of flying a leg of 145 km in length above a stratiform cloud layer located approximately 345 km west of the airfield on Coronado Island, San Diego. Although the CAR reflectance measurements at 1.64 and 2.20 μm were saturated for this high sun case (solar zenith angle $\theta_0 \approx 23°$), a comparison of measurements at 0.75 μm reveals agreement between the MCR and CAR to within 2%. Further comparisons with the TM onboard the Landsat-5 satellite show that the MCR measurements at 1.65 and 2.16 μm, and the CAR measurements at 0.75 μm, agree with the TM to within 2% and 7%, respectively. Based on these comparisons, we surmise that uncertainties introduced by mirror reflection, which primarily affects the calibration of the MCR near 0.75 μm, and the use of neutral density filters, which primarily affects the calibration of the CAR, can be neglected. Finally, we conclude that the accuracy of the radiometric calibration of MCR channels 1 (0.75 μm), 5 (1.65 μm) and 6 (2.16 μm), used for the analyses in the present investigation, is near that of the sphere calibration itself, estimated to be 5%–7%. We have further found it necessary to increase the intensity of TM band 2(0.56 μm) by 7% in order to bring it into closer agreement with comparable reflectance measurements from the MCR and CAR.

In addition to the MCR, we have made use of bands 2 and 7 of the Landsat-5 TM radiometer, images of which cover an area approximately 180 km × 170 km with a spatial resolution of 28.5 m. Since the critical spatial scale for measuring cloud amount is of the order of 250 m (Wielicki and Parker 1989), corrections for partially filled fields of view are not required when interpreting measurements from the MCR or TM.

3. Theoretical background

The method for inferring the optical thickness and effective particle radius of stratiform cloud layers described in Part I has been applied to multispectral images of the reflection function obtained with the MCR and TM during the FIRE marine stratocumulus IFO. In order to implement this procedure, computations of the reflection function were required for the standard problem of a plane-parallel homogeneous cloud layer with scaled optical thickness $\tau_c' = (1 - g)\tau_c = 0.4, 0.8, 1.2$ and ∞ and $r_e = 2^{(n+1)/2}$ for $n = 1, \cdots, 9$, where τ_c is the cloud optical thickness, g the asymmetry factor, and r_e the effective radius (see Part I for details). These computations were performed using the wavelengths and refractive indices summarized in Table 2, which are based on the refractive indices of water tabulated by Palmer and Williams (1974) for $\lambda \leq 1.65$ μm and Downing and Williams (1975) for $\lambda > 2.0$ μm, with some adjustment of the optical constants required for TM band 7 due to the large bandwidth of this channel.

In all analyses to be presented below, we allowed for water vapor absorption above the clouds as well as surface reflection below the clouds. For the water vapor absorption, we assumed the upper atmosphere had a column loading of water vapor $w_g = 0.6$ g cm^{-2} and computed the transmission as a function of solar zenith angle for nadir observations using LOWTRAN 5 (Kneizys et al. 1980). Although these computations necessarily show some dependence on solar zenith (and observational zenith) angle, we simply used the water vapor transmission values given in Table 2, which strictly apply when $\theta_0 \approx 35°$. Aside from this minor correction for water vapor transmission above the cloud layer, all reflection function measurements were analyzed using the exact values of the solar zenith angle,

TABLE 2. Spectral characteristics and optical properties of clouds for the Multispectral Cloud Radiometer (MCR) and Landsat-5 Thematic Mapper (TM) used during the July 1987 FIRE experiment. A_g represents the surface albedo of the ocean and T_w the transmission by water vapor above the cloud.

Radiometer	Channel	Central wavelength (μm)	Spectral resolution (μm)	Index of refraction	A_g	T_w
MCR	1	0.754	0.001	$1.332-0.0i$	0.060	1.00
	5	1.645	0.054	$1.317-7.83 \times 10^{-5}i$	0.050	1.00
	6	2.160	0.085	$1.294-3.50 \times 10^{-4}i$	0.045	0.95
TM	2	0.560	0.082	$1.333-0.0i$	0.060	1.00
	7	2.216	0.252	$1.291-4.50 \times 10^{-4}i$	0.045	0.90

viewing zenith angle, and azimuth angle between the sun and the viewing direction of the pixel at the time of the observations.

In order to interpret reflection function measurements for cloud optical thickness and effective radius, it is also important to include the effects of surface reflection, especially for optically thin clouds. For our analyses, which apply to marine stratocumulus clouds overlaying an ocean surface, we assumed the surface reflects radiation according to Lambert's law with surface albedos summarized in Table 2. These albedos, which were estimated from theoretical calculations, are in close agreement with measurements obtained by the CAR under overcast conditions (King et al. 1990), as discussed in the Appendix.

4. Results from observations on 10 July 1987

On 10 July the ER-2 and C-131A flew a tightly coordinated mission in which the ER-2 flew above and the C-131A within an extensive marine stratocumulus cloud layer located approximately 355 km from Coronado Island, San Diego. This mission, which consisted of continually flying legs ~ 145 km in length, represents the best flight coordination of the high-altitude ER-2 measurements with simultaneous in situ microphysical and radiation measurements obtained during FIRE. We will now present and discuss our analysis of the reflected solar radiation measurements acquired by the MCR between 0939 and 0951 PDT (flight line 4). Figure 1 illustrates a GOES-6 visible image taken at 1015 PDT on this day, upon which is superimposed the location and direction of flight of the ER-2.

Figure 2 illustrates corresponding images of the cloud optical thickness $\tau_c(0.75\ \mu m)$ and effective particle radius r_e derived from MCR measurements obtained during flight line 4. In both of these images, the aircraft was flying from top to bottom down the center of the images with the MCR scanning counterclockwise. Both of these images were remapped to a horizontal grid at 1 km altitude, thus providing a uniform spatial scale

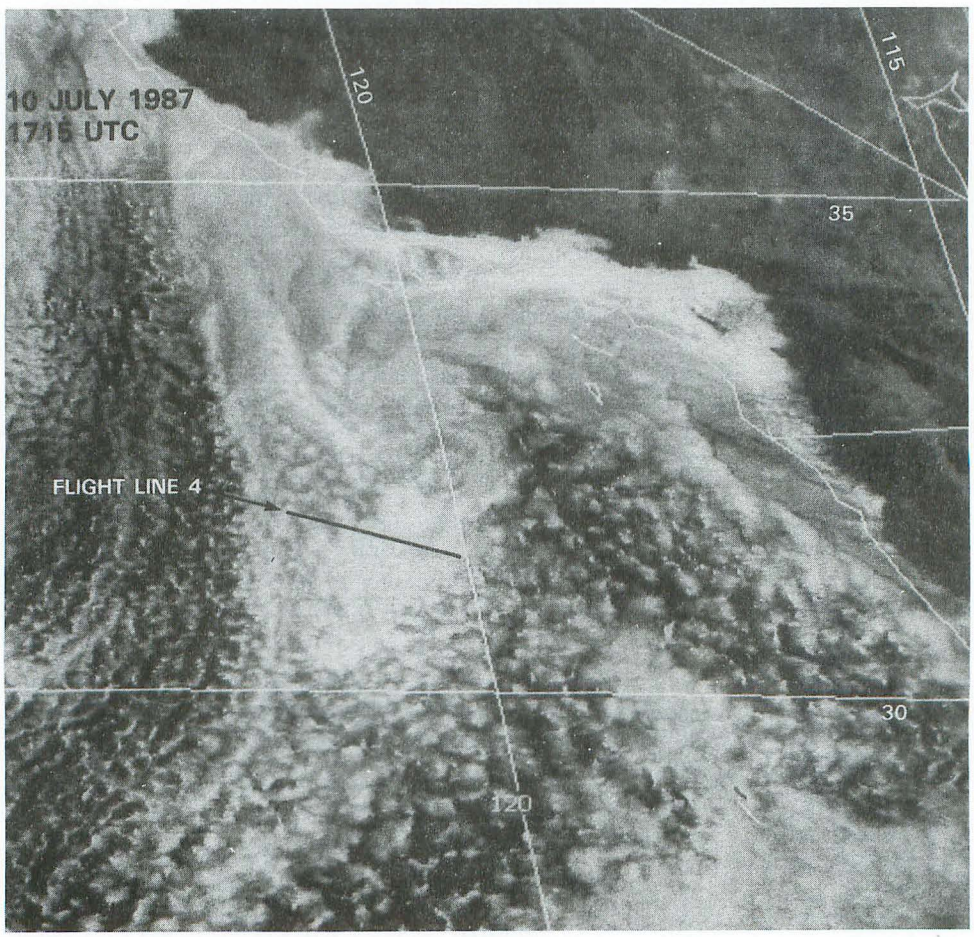

FIG. 1. GOES-6 visible image for 1715 UTC (1015 PDT) on 10 July 1987. The image encompasses the FIRE marine stratocumulus area covered by the Multispectral Cloud Radiometer measurements, and includes the flight track of the ER-2 observations. The arrow denotes the direction of flight.

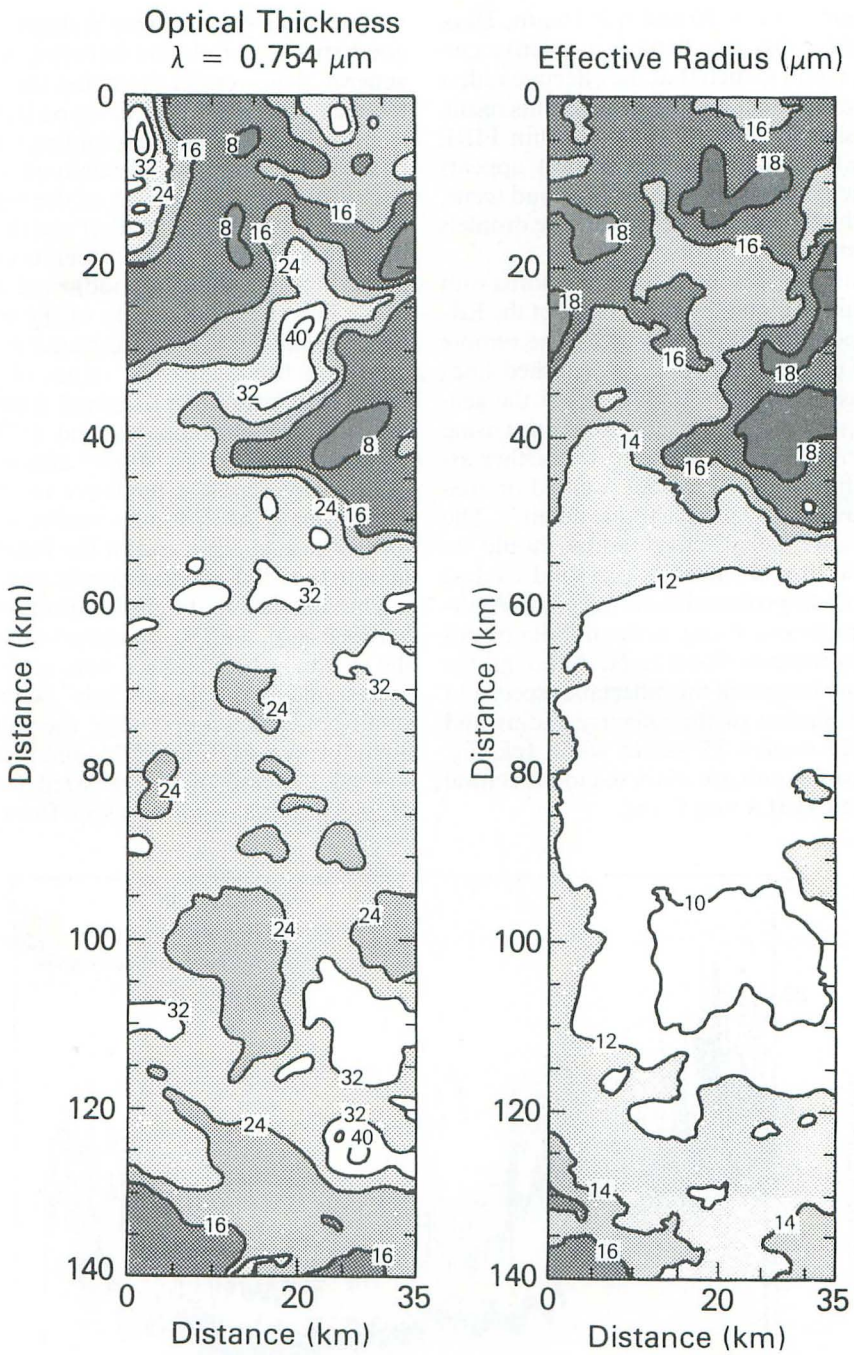

FIG. 2. Images of the cloud optical thickness and effective radius derived from 2465 scan lines of the MCR on 10 July 1987, flight line 4. These images have been remapped onto a horizontal grid at 1 km altitude, roughly corresponding to the cloud top altitude of the clouds in the scene.

over the 140 km × 35 km size of the images. These results, obtained using the two channel (0.75 and 2.16 μm) method described in Part I, have been contrasted with results obtained using the three channel (0.75, 1.65 and 2.16 μm) method. In general, we found that the results obtained by these two methods agree to within 4%, and thus have restricted our presentation to results obtained with the two channel method only.

Comparing the images of Fig. 2 with the GOES-6 image of Fig. 1, we find that the saturated parts of Fig. 1 correspond to $\tau_c \geq 24$ and $r_e \leq 14$ μm, and that the dark parts of the scene near the western end of the

flight line correspond to $\tau_c \leqslant 16$ and $r_e \geqslant 16$ μm. Thus, for this scene and for this day, there is a negative correlation between τ_c and r_e such that the effective radius increases as the optical thickness decreases. This result, which contrasts sharply with all optically thin FIRE data cases that we have examined (see below), appears to be related to the maritime nature of this cloud scene, which contains a high concentration of drizzle droplets and a large dispersion of droplet sizes.

Figure 3 compares the retrieved effective radius with in situ values obtained along the nadir track of the ER-2 aircraft as a function of flight distance. The remote sensing values of effective radius r_{remote} (dashed line) have been adjusted to the expected values at the geometric center of the cloud deck r_{center} (solid line) using the method described in Part I, where we further assumed vertical inhomogeneity model A based on marine stratocumulus clouds (see Part I for details). The center-adjusted values of effective radius should be compared with the in situ values $r_{\text{in situ}}$ (solid circles) derived from the PMS probes aboard the C-131A aircraft, which was primarily flying in the middle of this 440 m thick stratocumulus cloud layer. Although the scanning radiometer images of the reflectance spectrum permit the determination of the effective radius and optical thickness in images 35 km in width (cf. Fig. 2), the in situ measurements are restricted to the central location where the C-131A was flying.

One of the most striking features of Fig. 3 is the very good spatial correlation between r_{center} and $r_{\text{in situ}}$. In general, these results show that the center-adjusted effective radius is similar in shape but noticeably larger in magnitude than corresponding values derived from in situ microphysical measurements. This is especially true in the central portion of the flight line where the effective radius is the smallest and the optical thickness the largest. In this region differences of up to 2.5 μm occur between the center-adjusted and in situ values of r_e. The gradual decrease of the effective radius between 50 and 100 km, illustrated in Fig. 3, is also apparent in the decreasing values of cloud absorption (similarity parameter) derived from the CAR using the diffusion domain method (King et al. 1990). Twomey and Cocks (1989) and Rawlins and Foot (1990) also report a tendency for remote sensing to overestimate the in situ-derived effective radius, in the former case by 40% and in the latter case, which pertains to the FIRE marine stratocumulus region, by 25%.

One noticeable difference in the spatial correlation between r_{center} and $r_{\text{in situ}}$ occurs around 40 km,where the in situ values show a noticeable peak. This peak corresponds to a cloud "hole" with correspondingly small optical thickness near the western edge of the flight line (cf. Figs. 1 and 2), and results from the substantial increase of drizzle-sized ($\geqslant$100 μm radius) droplets in this region. As seen from Figs. 2 and 3 the

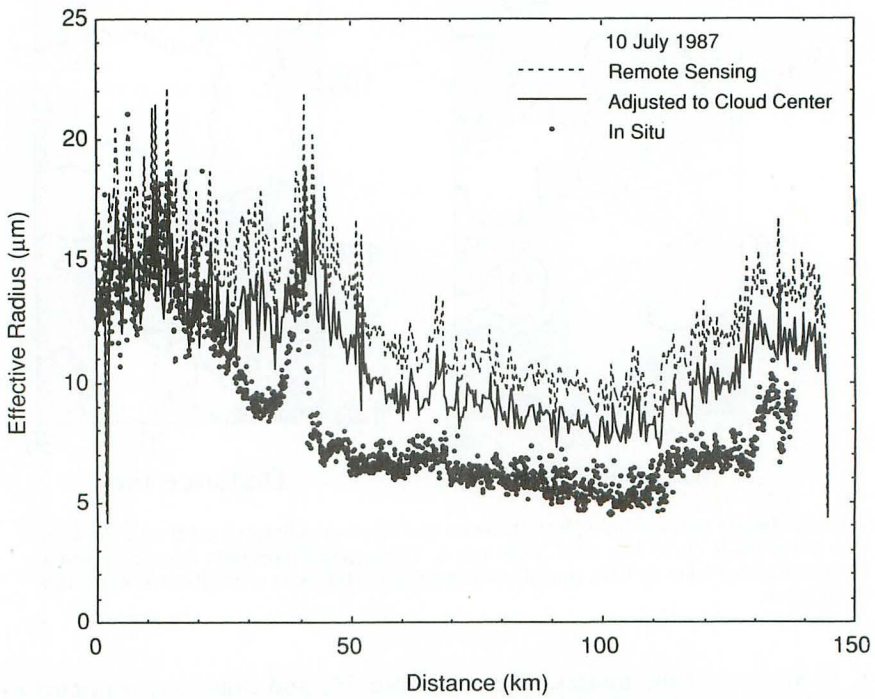

FIG. 3. Comparison of the effective radius as a function of distance along the nadir track of the ER-2 as derived from remote sensing (dashed line) and in situ measurements (solid circles). The solid line represents the expected values of effective radius at the geometric center of the cloud layer, derived from the remote sensing measurements by allowing for vertical inhomogeneity of droplet radius.

effective radius derived from the reflectance spectrum increases in a broad area around 40 km, but is somewhat less dramatic and striking than the in situ measurements. Since the sharp increase in $r_{\text{in situ}}$ is due to increased numbers of drizzle droplets low in the cloud, the reflectance spectrum, which is sensitive primarily to the cloud droplets in the upper 20% of the cloud, is relatively insensitive to the occurrence of drizzle near cloud base. The images of Fig. 2 suggest, however, that these clouds did have substantial drizzle near 40 km, especially on the left-hand side of the nadir track (cross track distances between 20 and 35 km), where values of r_{remote} in excess of 18 μm were found to occur.

Figure 4 compares the remote sensing optical thickness τ_{remote} (solid line) obtained along the nadir track of the ER-2 aircraft with corresponding estimates derived from in situ microphysical measurements $\tau_{\text{in situ}}$ (solid circles). In this case, the in situ values of cloud optical thickness have been estimated as follows:

$$\tau_{\text{in situ}} \approx \frac{3}{2\rho}\int_{z_b}^{z_t}\frac{w(z')}{r_e(z')}\,dz' \approx \frac{3}{2\rho}\frac{W_{\text{in situ}}}{r_{\text{in situ}}}, \quad (1)$$

where

$$W_{\text{in situ}} \equiv \int_{z_b}^{z_t} w(z')dz' \approx w_{\text{JW}}\Delta z. \quad (2)$$

In these expressions ρ is the density of water, w the cloud liquid water content, a function of altitude z, z_b and z_t the cloud base and cloud top heights, respectively, $W_{\text{in situ}}$ the liquid water path of the cloud, w_{JW} the liquid water content measured with the Johnson-Williams (JW) hot wire probe within the cloud layer, and Δz the effective cloud thickness allowing for the fact that the liquid water content is reduced near cloud top due to entrainment and that the measurements are not necessarily made at the geometric center of the cloud layer. These expressions, which are based in part on the assumption that the extinction efficiency factor equals 2, can be shown to overestimate the cloud optical thickness by $\approx$7% if we further make the realistic assumptions that the effective radius and liquid water content increase linearly with height, that the effective radius at cloud base is $\approx$57% of that at cloud top, and that the in situ measurements are made near the geometric center of the cloud layer (see Part I for details).

We have determined $W_{\text{in situ}}$ from an application of Eq. (2) to the $w(z)$ measurements obtained on each day during the profile ascents or descents summarized in Table 1. The effective geometric thickness Δz has been determined from these results by dividing by the w_{JW} measurements obtained at the profile level at which the horizontal flight legs were previously flown (cf. Table 1). The values of Δz thus obtained, together with the cloud top and cloud base heights and mean solar zenith angle at the time of the observations, are summarized in Table 3. These values of Δz were subsequently used to obtain estimates of $\tau_{\text{in situ}}$ and $W_{\text{in situ}}$

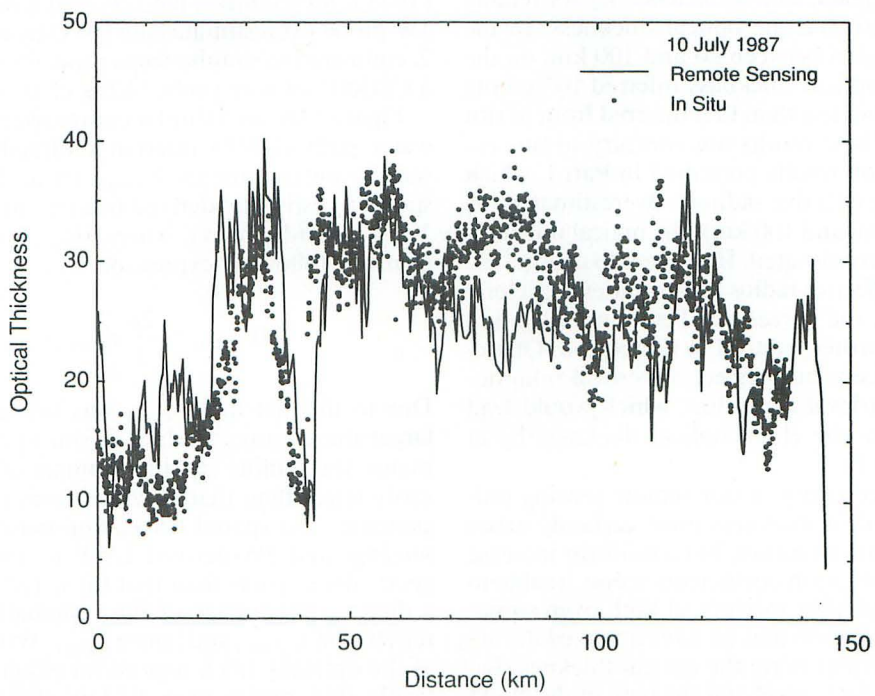

FIG. 4. As in Fig. 3 except for the cloud optical thickness, where the results obtained by remote sensing (solid line) are contrasted with estimates obtained from in situ liquid water content measurements obtained with the Johnson-Williams hot wire probe (solid circles).

TABLE 3. Approximate values of the solar zenith angle, cloud base altitude, cloud top altitude, effective geometrical thickness of the cloud layer, and mode optical thickness and standard deviation of the log-normal distribution which yields the best fit to the marginal probability density function of optical thickness defined by Eq. (4).

Date	θ_0	z_b (m)	z_t (m)	Δz (m)	τ_m	σ	Comment
7 July	29°	480	660	125	10.1	0.234	
10 July	46°	490	930	400	27.1	0.175	Main peak
13 July	30°	340	540	170	16.0*	0.209*	Eastern part
	28°	330	640	390			Western part
16 July	31°	480	770	280	27.7	0.268	

* Pertains to entire MCR image.

from time series of w_{JW} and $r_{\text{in situ}}$ obtained on the horizontal flight legs summarized in Table 1, where we have made use of Eqs. (1) and (2). The clouds measured on 13 July had a large variation in geometric thickness between the eastern and western portions of the cloud layer. For the western portion the C-131A flew near cloud base, so that the value of Δz is significantly larger than the true geometric thickness $z_t - z_b$.

Returning to Fig. 4 we find that the remote sensing values of optical thickness are similar in both shape and magnitude to corresponding estimates derived from in situ microphysical measurements. Near the beginning of the flight line and near 40 km, locations for which r_{center} and $r_{\text{in situ}}$ are is especially good agreement (cf. Fig. 3) and where there is a high concentration of drizzle droplets, the agreement between τ_{remote} and $\tau_{\text{in situ}}$ is quite good, with some tendency for remote sensing to overestimate the optical thickness. In the optically thick region between 50 and 100 km, on the other hand, the optical thickness inferred by remote sensing is somewhat less than that inferred from in situ measurements. These results are contrary to our expectations based on results presented in Part I, which showed that if the effective radius is overestimated (as in Fig. 3 between 50 and 100 km), the optical thickness should also be overestimated. If we were to assume the in situ values of effective radius in our retrieval of cloud optical thickness, the agreement between τ_{remote} and $\tau_{\text{in situ}}$ would be further reduced in this region. Of secondary importance is our neglect of vertical inhomogeneity in our retrieval algorithm, which would lead us to overestimate the cloud optical thickness by at most 3% (cf. Part I).

The largest uncertainty in our remote sensing estimate of cloud optical thickness most certainly arises from calibration uncertainties, but a uniform increase or decrease in calibration coefficients seems unable to account for the complex mixture of both overestimation and underestimation that we have observed during this flight line. Furthermore, the optical thickness between the aircraft flight level and the base of the cloud can be estimated from relative angular intensity measurements deep within a cloud layer. These results, necessarily independent of instrument calibration, have been obtained from the C-131A with the CAR at distances between 50 and 100 km of Fig. 4 (King et al. 1990, Fig. 10). The optical depths thus obtained are approximately 40%–50% of those inferred from our nearly simultaneous reflected solar radiation measurements, thereby enhancing our confidence that the C-131A was flying near the middle of this cloud layer and that the optical thickness values obtained by remote sensing are quite accurate.

Due to the indirect nature of our estimate of $\tau_{\text{in situ}}$, including uncertainty in the JW measurements as well as uncertainty in the geometric thickness of the cloud layer, which we assume to be constant during a horizontal flight leg, we suspect that considerable uncertainty lies in our estimates of cloud optical thickness from in situ microphysical measurements. Knollenberg (1981), for example, has reported a case in which the JW probe overestimates the LWC by a factor of about 2, compared to simultaneous measurements made with a CSIRO hot wire probe (King et al. 1978).

Figure 5 shows a similar comparison between liquid water path (LWP) inferred indirectly from remote sensing measurements W_{remote} (solid line) and corresponding estimates derived from in situ measurements $W_{\text{in situ}}$ (solid circles), where W_{remote} was determined from the following expression:

$$W_{\text{remote}} = \frac{2\rho}{3} \tau_{\text{remote}} r_{\text{center}}. \tag{3}$$

Due to the fact that τ_{remote} was similar to, and r_{center} larger than, corresponding in situ microphysical estimates, the remote sensing estimate of LWP is necessarily larger than that obtained from the JW hot wire estimate. The spatial correlation between the remote sensing- and JW-derived LWP is nevertheless quite good, albeit worse than that for τ_c (cf. Fig. 4). This is a direct consequence of the systematic errors in our retrieval of r_{remote}, and hence r_{center}. With the exception of the optically thick regions on either side of the optically thin region near 40 km, differences between W_{remote} and $W_{\text{in situ}}$ are generally $\leqslant 50$ g m^{-2}. Larger discrepancies occur on either side of this optically thin region due primarily to the fact that our retrieval of

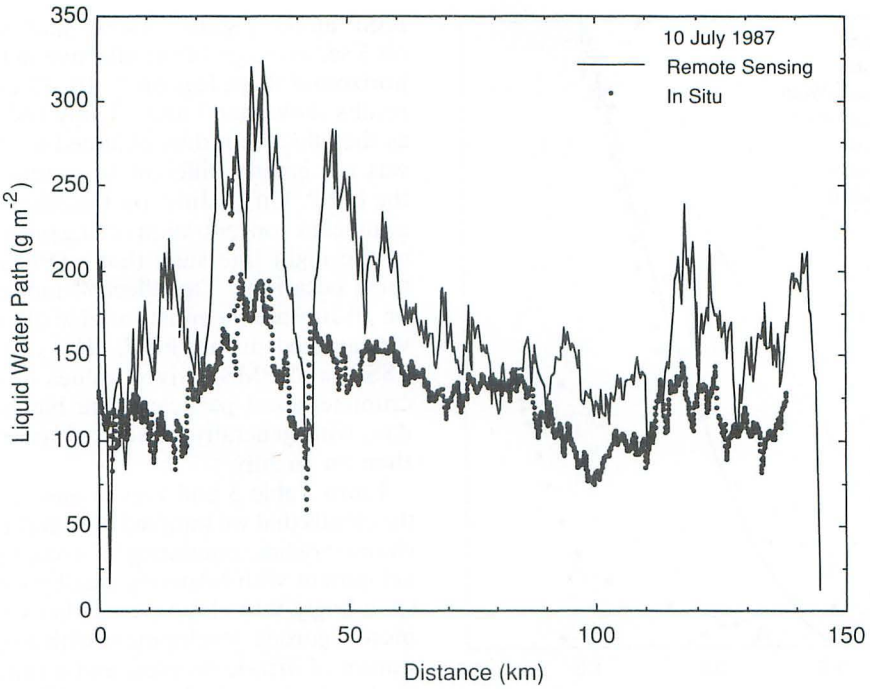

FIG. 5. As in Fig. 4 except for the liquid water path.

r_{remote} and r_{center} was generally much broader in this region than that derived from in situ measurements (cf. Fig. 3). This is most likely a consequence of the fact that the C-131A aircraft was displaced somewhat off the nadir track of the ER-2 aircraft, and that the width of this large droplet region was much broader on the left-hand side of the ER-2 than on the right-hand side (cf. Fig. 2).

Corresponding estimates of the LWP derived from the PMS probes (not illustrated) do not show such a sharp dip of LWP in the vicinity of 40 km. Although the magnitude of the liquid water content derived from integrations of PMS-derived size distribution measurements was significantly lower than corresponding measurements obtained with the JW probe, consistent with the findings of Personne et al. (1982) and Baumgardner et al. (1985), these measurements are nevertheless sensitive to drizzle-sized droplets for which remote sensing and JW measurements are insensitive. Thus the apparent agreement between W_{remote} and $W_{\text{in situ}}$ at 40 km appears to be partially due to an insensitivity in both techniques to the presence of substantial concentrations of drizzle droplets.

5. Microphysical properties of marine stratocumulus clouds

In addition to the level flight leg of 10 July, described in the previous section, we obtained measurements of the vertical distribution of cloud microphysics from a number of C-131A ascents and descents on four days during FIRE (cf. Table 1). Table 3 summarizes the cloud top and cloud base altitudes for each of these profiles.

Figure 6 shows vertical profiles of the normalized effective radius $\hat{r} = r_e(z)/r_t$ as a function of normalized optical depth $\hat{\tau} = \tau/\tau_c$ for five different profiles and for the two inhomogeneous models defined in Part I, where r_t is the effective radius at cloud top and τ is determined by assuming the extinction efficiency factor equals 2 and integrating the ratio of the liquid water content to effective radius as a function of height [as in Eq. (1)]. On 13 July we obtained microphysical profiles in both the eastern and western portions of the flight leg, with the western part being optically and geometrically thicker than the eastern part. The normalized effective radius profiles on 7 and 13 July, as well as the upper half of the profile on 10 July, agree quite well with inhomogeneous model A (solid line), based on in situ microphysical measurements obtained from the UK C-130 aircraft during FIRE (Albrecht et al. 1988). On 10 July larger particles were present in the lower half of the cloud layer, suggesting a two layer structure in which the lower layer contained more large, drizzle-sized droplets. On 16 July large droplets were present both near cloud top and near cloud base, with much smaller droplets in the middle of the cloud layer.

From these results we conclude that a vertical adjustment to r_{remote} based on inhomogeneous model A is a reasonable correction for cloud vertical inhomogeneity on 7 and 13 July. Since reflected solar radiation measurements are primarily sensitive to the micro-

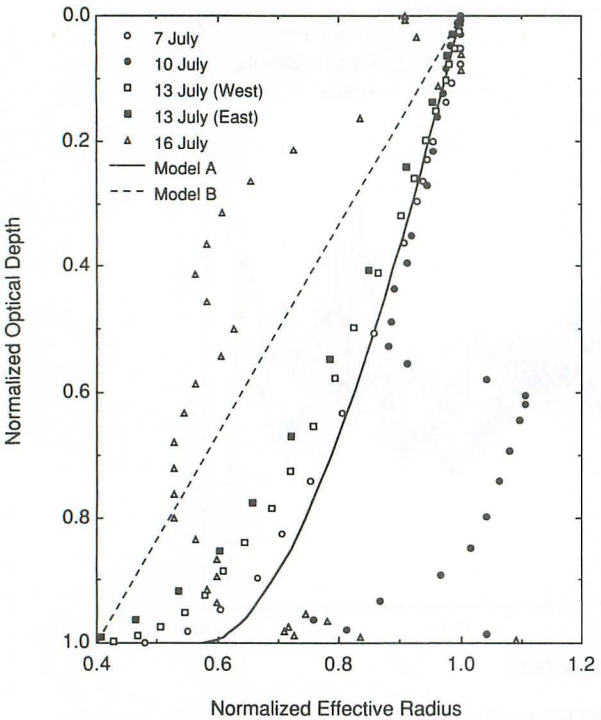

FIG. 6. Profiles of effective radius, relative to the value at cloud top, as a function of optical depth, relative to the total optical thickness of the cloud layer. The data points were derived from measurements in marine stratocumulus clouds. The solid and dashed curves correspond to models A and B used to simulate the effects of vertical inhomogeneity on the retrieval of cloud optical thickness and effective radius (see Part I for details).

physical properties of clouds at an optical depth 20%–40% of the total optical thickness of the cloud layer, as demonstrated in Part I, and are largely insensitive to the microphysical properties near cloud base, an application of our vertical adjustment technique based on model A is expected to overestimate the effective radius at the geometric cloud center r_{center} on 16 July. On 10 July it is very difficult to access the error in r_{center} that results from an application of model A, since the vertical profile of effective radius undergoes a large deflection near cloud center on this day. This westbound descending profile was obtained between flight track distances of 64.5 and 50.6 km of Figs. 2–5, and thus the large increase in droplet size near cloud base may have been influenced by the drizzle-sized droplets near 40 km, discussed in the foregoing section.

The concentration and size distribution of drizzle droplets ($r \geq 100$ μm) is also a significant indicator of the airmass regime of stratocumulus clouds (Albrecht 1989; Radke et al. 1989). Since the FSSP probe is not sensitive to drizzle-sized droplets, the presence of drizzle can most readily be assessed by comparing the effective radius obtained by integrating the size distribution measurements obtained using all three PMS probes with comparable results obtained using the FSSP alone. Figure 7 shows such scatter plots based on 5 sec averages of the effective radius obtained from horizontal flight legs on 7, 10, 13 and 16 July. These results show that 7 and 13 July had very little drizzle, as the effective radius obtained using all PMS probes was not greatly different from results obtained using the FSSP. On 16 July, on the other hand, there was a significant concentration of drizzle droplets on portions of the flight line such that $r_e(\text{PMS}) > r_e(\text{FSSP})$ on these occasions. The effective radius results obtained on 10 July are the most variable of any of the days that we sampled during FIRE. The contrast between the FSSP- and PMS-derived values of r_e imply that micrometer-sized particles were highly variable on this day, with generally smaller concentrations of drizzle than on 16 July.

From Table 3 and Figs. 6 and 7, we conclude that the clouds that we sampled on 7 and 13 July had similar characteristics, consisting of comparatively weak development with relatively small particles and a correspondingly thin cloud deck, whereas 10 and 16 had a more vigorous development with a significant concentration of drizzle droplets and a much larger geometrical and optical thickness. Although many past studies have been based on the FSSP probe alone, it is obvious from our results that it is necessary to take into account the full spectrum of droplet sizes, which requires measurements using the OAP cloud and precipitation probes in addition to the FSSP.

6. Comparison between remote sensing and in situ observations

Figure 8 compares the center-adjusted effective radii derived from remote sensing observations with comparable values obtained from nearly simultaneous in situ microphysical measurements obtained from the C-131A aircraft. We have excluded from this comparison all data for which $\tau_c \leq 3$, optically thin clouds for which our retrieval is believed to be the least reliable. The remote sensing observations in the panel on the left were derived from ER-2 MCR measurements on 7, 10 and 13 July, while the panel on the right was derived from Landsat-5 TM measurements on 16 July. This was necessitated by the fact that the ER-2 aircraft was not collocated with the C-131A aircraft on 16 July, although both aircraft were well within the Landsat-5 scene. Since the stratocumulus cloud layer on this day was optically thick, comparable to 10 July (see below), the TM measurements in band 2 were largely saturated. Thus our retrievals of r_{remote} and the corresponding correction of r_{remote} to r_{center} were necessarily indirect, requiring us to estimate the cloud optical thickness from in situ measurements of the liquid water content and effective radius [as in Eq. (1)].

From these comparisons between remote sensing and in situ values of effective radius, we conclude that r_{center} is typically 2–3 μm larger than $r_{\text{in situ}}$, with little

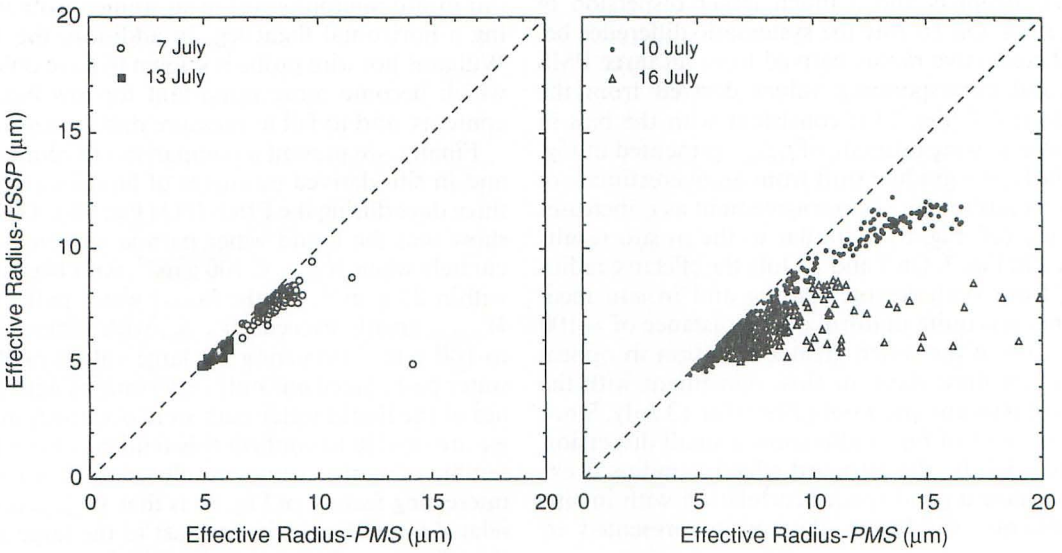

FIG. 7. Comparison of the effective radius derived from all three PMS probes (FSSP-100, OAP-200X and OAP-200Y) with corresponding results obtained with the FSSP alone.

sensitivity to particle radius, provided $r_{\text{in situ}} \leqslant 9$ μm. For particles larger than about 10–11 μm, we observe a gradual tendency for remote sensing to underestimate the effective radius. This result, which is particularly evident on 16 July, can be explained by the fact that any remote sensing method based on reflected solar radiation measurements is necessarily insensitive to large concentrations of drizzle droplets in the lower half of the cloud layer. In fact, one could argue that the reflection properties of clouds are largely determined by the size of the cloud droplets in the upper 20%–40% of the cloud layer, and as such this inability to sense the presence of large particles low in the cloud is unimportant for climate applications involving the radiation budget at the top of the atmosphere.

This explanation for the gradual departure of r_{center} from $r_{\text{in situ}}$ as the effective radius increases is confirmed by comparing Fig. 8 with the in situ microphysical measurements presented in Fig. 7. These results show that 7 and 13 July had very few drizzle droplets with a correspondingly small dispersion of effective radius, whereas 10 and 16 July had a significant concentration

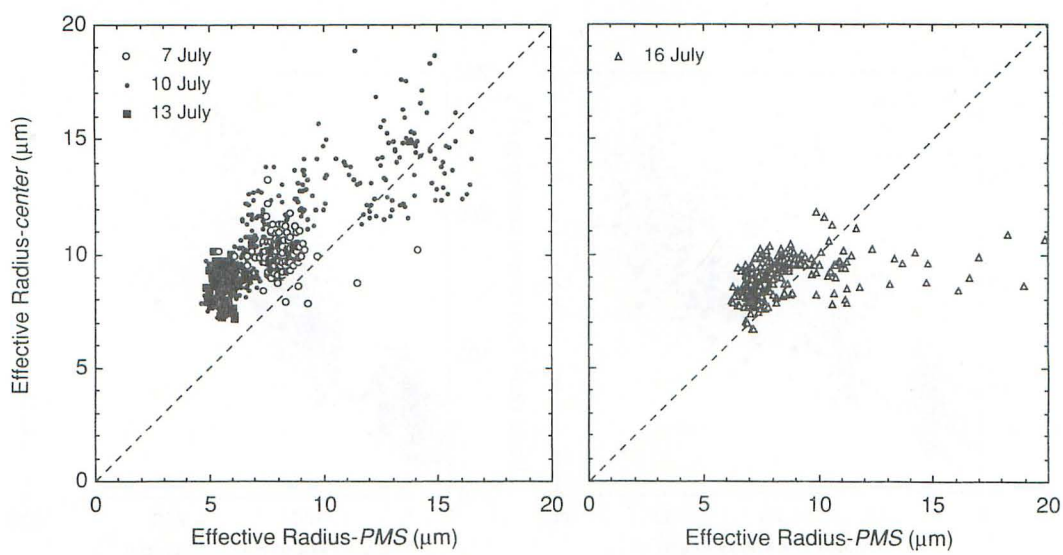

FIG. 8. Comparison of the effective radius r_{center} derived from remote sensing with comparable values obtained from in situ microphysical measurements obtained using all three PMS probes ($r_{\text{in situ}}$). The panel on the left was obtained from analysis of ER-2 MCR measurements and the panel on the right from Landsat-5 TM measurements.

of drizzle droplets and a much larger dispersion of droplet sizes. On 16 July the systematic difference between the effective radius derived from all three PMS probes and corresponding values derived from the FSSP alone (cf. Fig. 7) is consistent with the bias in our remote sensing estimate of r_{center}, presented in Fig. 8. Similarly, the gradual shift from an overestimate of effective radius to one of close agreement as r_e increases on 10 July (cf. Fig. 8) is similar to the in situ results presented in Fig. 7. On 7 and 13 July the effective radius derived from both remote sensing and in situ measurements was quite uniform over a distance of $\approx$100 km, in spite of the much greater variation in optical thickness on these days, in close agreement with the findings of Rawlins and Foot (1990) for 13 July. Since the scatter plots of Fig. 7 also show a small dispersion on 7 and 13 July, the retrieved effective radius is expected to have a good spatial correlation with in situ measurements, similar to the results presented in Fig. 3.

Figure 9a shows a comparison between the cloud optical thickness derived from MCR reflectance measurements and corresponding values obtained from an application of Eqs. (1) and (2) to nearly simultaneous in situ microphysical measurements. These results indicate that the cloud optical thickness is in reasonably close agreement to in situ estimates, with 90% of data points falling within the region $|\tau_{\text{remote}} - \tau_{\text{in situ}}| \leqslant 10$. Furthermore, the optical thickness appears to be overestimated when $\tau_{\text{in situ}} \leqslant 10$ and to be underestimated when $\tau_{\text{in situ}} \geqslant 20$, consistent with the results presented in Fig. 4. The largest uncertainty in these optical thickness comparisons most likely arises from uncertainties in estimating $\tau_{\text{in situ}}$, rather than τ_{remote}, since considerable uncertainty lies in our estimate of the effective geometric thickness of the cloud layer to be applied to our in situ microphysical measurements obtained during a horizontal flight leg. In addition, the Johnson-Williams hot wire probe is known to have offset errors, which become more important for low liquid water contents, and to fail to measure drizzle-sized droplets.

Finally, we present a comparison of remote sensing and in situ-derived estimates of liquid water path for three days during the FIRE IFO (Fig. 9b). These results show that the liquid water path is retrieved quite accurately when $W_{\text{in situ}} \leqslant 100$ g m^{-2}, with biases typically within 25 g m^{-2}. As the liquid water path increases, W_{remote} greatly exceeds $W_{\text{in situ}}$, with differences of up to 100 g m^{-2} occurring for large values of the liquid water path. Since our only observations with large values of the liquid water path were obtained on 10 July, we are unable to confirm this tendency for a large ensemble of marine stratocumulus clouds. An especially interesting feature of Fig. 9b is that W_{remote} is well correlated with $W_{\text{in situ}}$, in contrast to the large scatter in the effective radius and optical thickness comparisons shown in Figs. 8 and 9a.

7. Statistical properties of marine stratocumulus clouds

Although some discrepancy remains between in situ and remote sensing estimates of τ_c, W and r_e, it is nevertheless worthwhile to examine the statistical properties of these variables for marine stratocumulus clouds, especially given the recent interest in parameterizing the shortwave radiative properties of clouds in terms of W and r_e (Slingo 1989). Figure 10a shows joint probability density functions of τ_c and r_e derived from MCR images on each of the four days of our observations during FIRE (cf. Table 1). The five contour lines for each day correspond to the 10, 30, 50, 70 and 90% occurrence levels, from which the mode

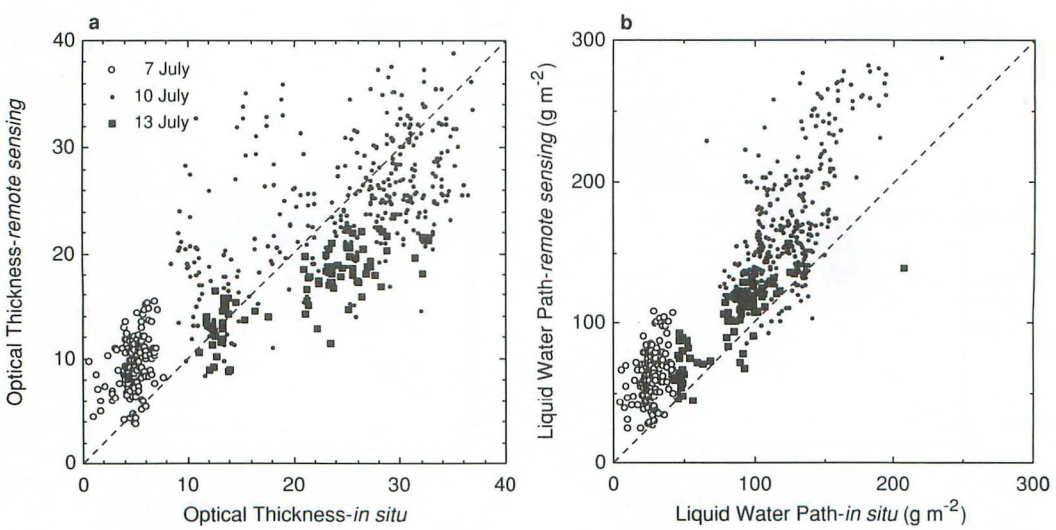

FIG. 9. Comparison of (a) optical thickness and (b) liquid water path derived from remote sensing with comparable values obtained from in situ microphysical measurements.

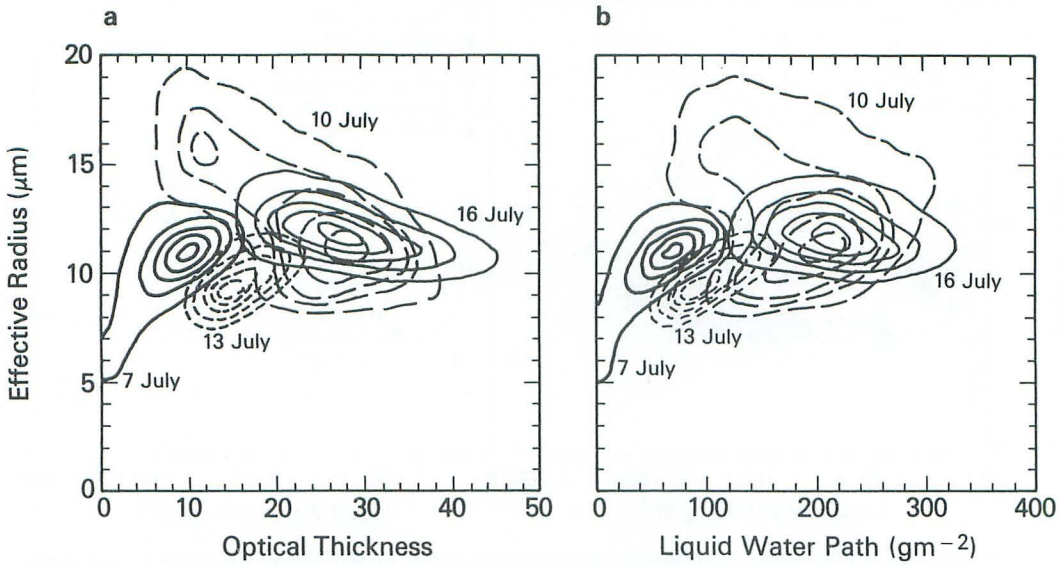

FIG. 10. Joint probability density functions of (a) the cloud optical thickness and effective radius, and (b) the liquid water path and effective radius, for four days during FIRE. These results were derived from MCR measurements acquired from the ER-2 aircraft, where the effective radius r_{remote} has not been adjusted to the geometric center of the cloud layer. The five contour lines for each day correspond to the 10, 30, 50, 70 and 90% occurrence levels.

values and interquartile ranges can readily be inferred. These results were obtained from MCR images 35 km in width and 105–165 km in length, depending on day, and are therefore not restricted to nadir observations as in our comparisons with in situ microphysical measurements. The effective radii presented here are the remote sensing values, and have thus not been adjusted to cloud center. Comparable results for W and r_e are presented in Fig. 10b, where the liquid water path W has been obtained from the remote sensing estimates of τ_c and r_e in an analogous manner to Eq. (3).

If we consider the composite properties of the cloud ensemble of four days as a single statistic, we ascertain little correlation between τ_c (or W) and r_e. In contrast, the statistical properties of a single day show a distinct positive correlation between τ_c (or W) and r_e on the optically thin days of 7 and 13 July, and a modest negative correlation on the optically thick days of 10 and 16 July. The negative correlation on 10 July is consistent with the results presented in Figs. 2–5, which showed the optically thick (thin) portions of the cloud scene had small (large) droplet radii. These results are compatible with the fact that the in situ microphysical properties of the clouds on 7 and 13 July were similar, and that these clouds differed in their microphysical properties from those of 10 and 16 July (cf. Figs. 7 and 8). Rawlins and Foot (1990) found a tendency for larger effective radii to be associated with clouds of greater optical thickness, consistent with our results for 7 and 13 July.

To examine this point further, we illustrate in Fig. 11 the relationship between W and r_e obtained from numerous in situ microphysical measurements, where the panel on the left pertains to C-131A observations during FIRE and the panel on the right to results reported by previous investigators. All of these measurements were acquired in marine stratocumulus clouds with the exception of those of Herman and Curry (1984), which were obtained in summertime arctic stratus clouds in Alaska. In addition to these observations, Fig. 11 illustrates the empirical relationship between W and r_e implicitly included in Stephens (1978) parameterization of the shortwave radiative properties of water clouds (dashed curve).

Although there are significant differences in the values of the liquid water path and effective radius inferred from in situ and remote sensing measurements, the in situ measurements presented in Fig. 11 enable us to gain further insight into the remote sensing results presented in Fig. 10. The in situ measurements generally fall into two categories, as in the remote sensing observations, with some results showing a weak positive correlation between W and r_e (7 and 13 July and a portion of 10 July) while others show a negative correlation (16 July and the optically thin, drizzle-dominated portion of 10 July). Together with Fig. 7 these results suggest that the joint probability density function of liquid water path and effective radius reflects very well the differences in the microphysical characteristics of two different airmass regimes, one with and the other without significant drizzle-sized droplets.

Once the joint probability density functions $f(\tau_c, r_e)$ and $f(W, r_e)$ have been determined, as in Figs. 10a and 10b, it is straight forward to compute the marginal probability density functions $f(\tau_c)$, $f(W)$ and $f(r_e)$. These results, presented in Figs. 12–14 respectively,

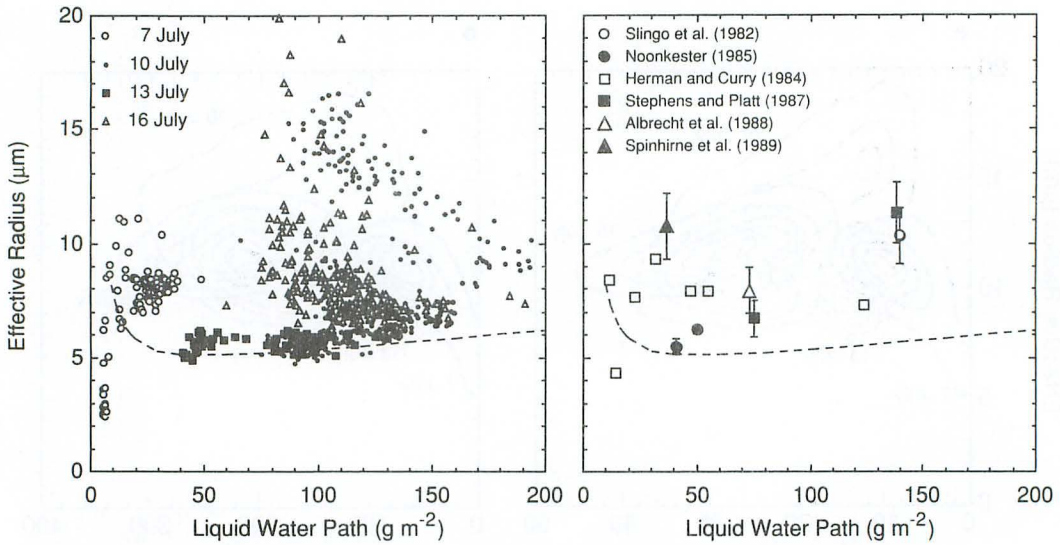

FIG. 11. Scatter plot of the liquid water path and effective radius derived from in situ microphysical measurements, where the panel on the left pertains to C-131A observations during FIRE and the panel on the right to results obtained by previous investigators. The dashed curve superimposed on these results is the empirical relationship presented by Stephens (1978).

were obtained from MCR images consisting of 30 000–45 000 pixels, depending on day, each of which had a spatial resolution of 120–170 m and was remapped onto a horizontal grid and sampled every 350 m (cf. Fig. 2). As seen on examination of Fig. 12, all of the marginal probability density functions of τ_c are monomodal, with the exception of 10 July, which has a secondary maximum for optically thin clouds. The portion of the cloud scene on this day that corresponds to small optical thicknesses also consists of large particles

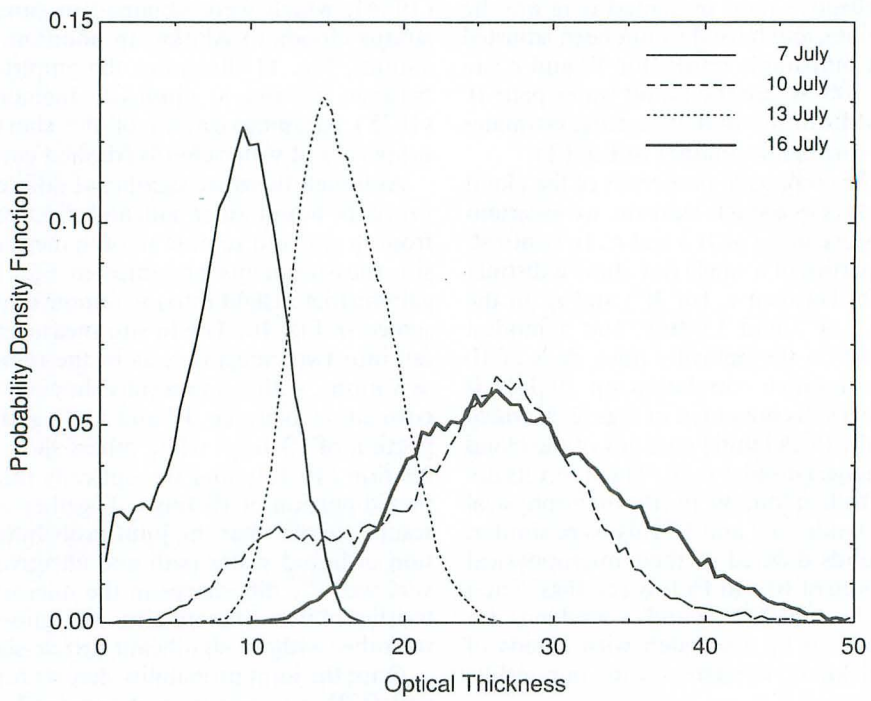

FIG. 12. Marginal probability density function of cloud optical thickness for four days during the FIRE marine stratocumulus IFO, derived from MCR measurements acquired from the ER-2 aircraft.

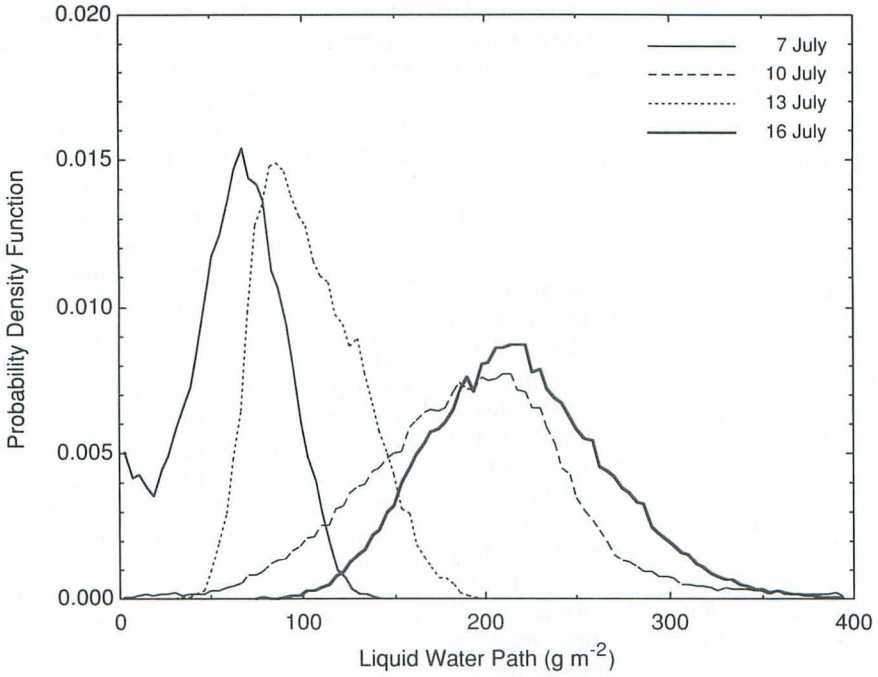

FIG. 13. As in Fig. 12 except for the liquid water path.

(cf. Figs. 3 and 4), thereby suggesting a two layer cloud structure with large particles low in the cloud (cf. Fig. 6). When the upper layer thins out, which occurs near the beginning of the flight line, the underlying layer having large particles is clearly observed. This may help explain why we detected relatively few drizzle droplets on this day in spite of the large variability in effective radius.

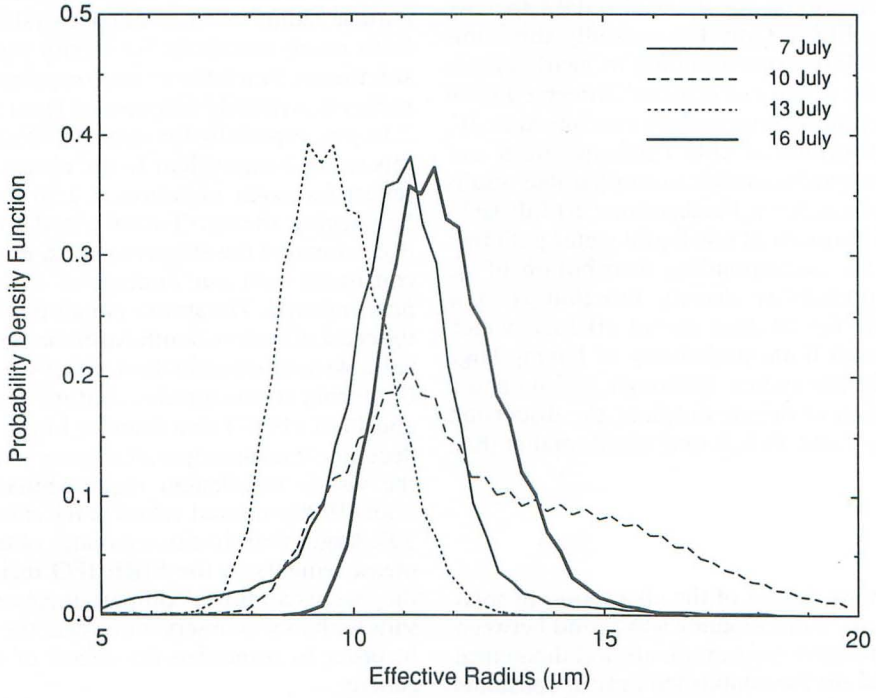

FIG. 14. As in Fig. 12 except for the effective radius, which has not been adjusted to the geometric center of the cloud layer.

There is some evidence that clouds have a fractal structure resulting in a marginal probability density function of τ_c very close to a log-normal distribution (Cahalan et al. 1989) of the form:

$$f(\tau_c) = \frac{1}{(2\pi)^{1/2}\sigma\tau_c} \exp[-(\ln\tau_c - \ln\tau_m)^2/(2\sigma^2)], \quad (4)$$

where τ_m is the mode optical thickness and σ the standard deviation of the probability density function. The values of τ_m and σ yielding the best fits to the distributions presented in Fig. 12 are summarized in Table 3. Lognormal distributions fit our experimental observations quite well, including the tails of the distributions, although a Gaussian distribution also fits the observations due to the narrow dispersion of optical thickness in our results. The mode optical thickness on 10 and 16 July was similar in magnitude and the largest that we observed ($\tau_m \approx 27$), while 7 July had the smallest mode optical thickness ($\tau_m \approx 10$). The dispersion of the probability density functions for all days that we observed during FIRE was quite small ($\sigma \approx 0.22$). These results are in stark contrast to the results obtained by Gorodetskiy et al. (1980) and King (1987), who found that the probability density functions of cloud optical thickness for the stratiform cloud layers that they observed were highly skewed, with a characteristic tail of the distributions extending to large values of τ_c.

The marginal probability density functions of liquid water path and effective radius, illustrated in Figs. 13 and 14, are monomodal for all of the days that we observed during FIRE. Only the optically thin (low W) portion of 7 July, corresponding to nearly cloud-free conditions for which our retrieval is deemed to be the least reliable, shows a secondary maximum in W. All of the distributions of $f(W)$ inferred from our analysis have a skewness similar to comparable results in the distributions of $f(\tau_c)$. Furthermore, 10 July lacks the secondary maximum at low liquid water path that was evident in the corresponding distribution of τ_c. The marginal probability density function $f(r_e)$ is nearly symmetric for all days except 10 July, which has a long tail with finite probability of having large values of the effective radius. Although 16 July had a large concentration of drizzle droplets, the dispersion itself is similar to 7 and 13 July and much smaller than 10 July.

8. Discussion

In many previous studies of the absorption of solar radiation by clouds, a discrepancy was found between broadband pyranometer measurements and theoretical calculations based on the established optical constants of water droplets and water vapor, as recently reviewed by Stephens and Tsay (1990). This discrepancy, often referred to as the "anomalous absorption paradox," has been attributed to a number of different hypotheses, each of which has a different consequence for the visible and near-infrared portions of the solar spectrum. This discrepancy between observations and theory led Twomey (1972, 1977) to suggest that absorbing aerosol particles, either within the droplets themselves or interstitial to them, may be partly responsible for this excess absorption. Calculations by Newiger and Bähnke (1981) showed that absorbing aerosol particles interstitial to the cloud droplets can enhance cloud absorption to values up to 30% of the incident solar radiation, and that this effect is largely restricted to wavelengths $\lambda \leqslant 1.5$ μm. The possibility also exists that leakage of radiation through the sides of clouds might account for some of the large values of absorption implied by the measurements (Welch et al. 1980; Ackerman and Cox 1981). Wiscombe et al. (1984) suggested that significant concentrations of large, drizzle-sized droplets could contribute to larger absorption values than typically obtained from calculations, but this effect would be largely restricted to wavelengths $\lambda \geqslant 1.5$ μm. Finally, Stephens and Tsay (1990) suggested that an unobserved water vapor continuum, if found to be present, might contribute to explaining this "anomalous absorption paradox."

In the present investigation we were unable to confirm the existence of any appreciable anomalous absorption in the visible wavelength region, as this would have led us to underestimate the optical thickness in our remote sensing analysis, contrary to our observations. In contrast, we inferred values of the effective particle radius in excess of comparable results obtained from nearly simultaneous in situ microphysical measurements. Since the remote sensing-derived effective radius is primarily determined from the reflectance at 2.16 μm, especially for optically thick clouds (Part I), this result is equivalent to the observation that clouds reflect *less* solar radiation at 2.16 μm than predicted by existing theory. Twomey and Cocks (1989) also overestimated the effective radius, in their case by 40%, consistent with our findings of darker clouds in the near-infrared. The stratus clouds that they observed off the coast of eastern South Australia were generally more variable and optically thicker ($10 \leqslant \tau_c \leqslant 128$) than the California stratocumulus that we observed. Stephens and Platt (1987) also found a lower near-infrared reflectance than anticipated, relative to measurements in the visible wavelength region. Finally, Rawlins and Foot (1990) inferred values of the effective radius 20%–50% larger than in situ estimates obtained from FSSP measurements in the FIRE IFO region. In their case they were careful to compare their remote sensing results with in situ observations near the top of the clouds in order to minimize the effects of vertical inhomogeneity.

In order to assess the overall uncertainties in the retrieved optical thickness and effective radius arising

from uncertainties in cloud absorption, we performed radiative transfer computations at 0.75 and 2.16 μm for vertically homogeneous, plane-parallel clouds. At each wavelength the reflection function was computed for $\theta_0 = 30°$, $\theta = 0°$, $\tau_c = 5$, 7.5, 10, 12.5, 17.5, 20, 30 and $r_e = 5$, 6, 7, 8, 10, 12, 16, 18 and 20 μm, corresponding to nadir observations at a solar zenith angle close to the bulk of our observations (cf. Table 3). For each of these conditions we introduced additional absorption to the clouds, from which we retrieved τ_c and r_e using our two-channel algorithm. The enhanced absorption models that we considered were 1) continuum gaseous absorption $\tau_g = 0.1$ and 0.2, introduced separately at 0.75 and 2.16 μm, and 2) droplet absorption at 2.16 μm with a refractive index $m = 1.294–0.0005i$, corresponding to an imaginary refractive index exceeding that of our benchmark model (cf. Table 2).

The results of these simulations are presented in Fig. 15, which shows the effects of enhanced absorption on the retrieval of cloud optical thickness (left) and effective radius (right). Figure 15a, which pertains to the case where $r_e = 8$ μm, shows that an introduction of an absorption optical thickness $\tau_g(0.75\ \mu\text{m}) = 0.1$ leads to an appreciable underestimation of the optical thickness by remote sensing, in contrast to the results of our observations, presented in Fig. 9a. Furthermore, these results show that introducing gaseous absorption at 2.16 μm has a negligible effect on the retrieval of cloud optical thickness, as anticipated from the results presented in Part I. The vertical error bars illustrated in Fig. 15a represent the range of retrievals of τ_{remote} that we obtained for the full range of effective radii included in our simulations ($5 \leq r_e \leq 20$ μm). Based on these findings, we conclude that an absorption optical thickness $\tau_g(0.75\ \mu\text{m}) = 0.1$ is too large to explain our optical thickness retrievals in the marine stratocumulus clouds that we observed in the FIRE IFO region.

Twohy et al. (1989) measured the mass mixing ratio of carbon particles in cloud water and found values ranging from 2 to 8 ($\times 10^{-8}$), which corresponds to an absorption optical thickness ranging from $0.00015Q_{\text{abs}}$ to $0.0006Q_{\text{abs}}$, where we further assumed that a typical radius of a carbon particle is 0.01 μm (probably as an inclusion in a larger particle) and that $W = 100$ g m^{-2}. The absorption efficiency factor of carbon particles (Q_{abs}) is necessarily less than 1, although its precise value depends significantly on how carbon particles are mixed with cloud droplets. Hence, unless we introduce a strong enhancement mechanism such as absorption of surface waves by carbon particles on the droplet surface (Chýlek et al. 1989), it seems impossible to have a visible absorption optical thickness as large as 0.1. This is also supported by the observations of King et al. (1990), who found a single scattering albedo at 0.75 μm of 0.9997, thereby implying an absorption optical thickness $\tau_a \ll 0.1$.

Figure 15b shows a corresponding assessment of the effect of enhanced absorption on the determination of the effective radius of cloud droplets. These simulations pertain to the case where the true optical thickness $\tau_c = 20$. Introducing gaseous absorption $\tau_g(0.75\ \mu\text{m}) = 0.1$ leads to an underestimation of the effective radius, in addition to an underestimation of the cloud optical thickness (cf. Fig. 15a), contrary to our results (Figs. 3 and 8) and those of Foot (1988), Twomey and Cocks (1989) and Rawlins and Foot (1990). The

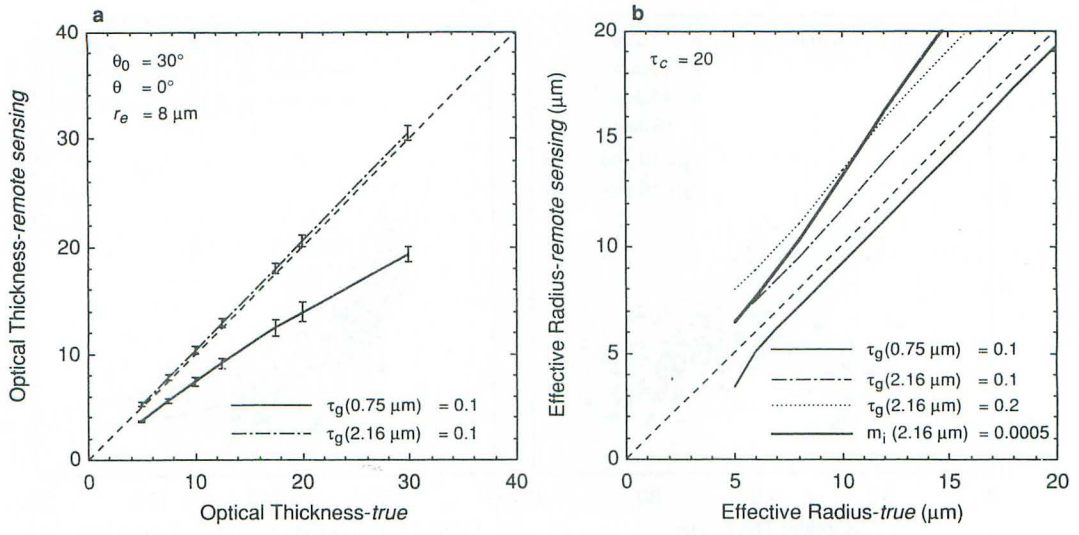

FIG. 15. Comparison of the (a) optical thickness and (b) effective radius derived from simulated remote sensing measurements in which enhanced absorption is introduced separately at 0.75 and 2.16 μm. These simulations, which pertain to nadir observations at $\theta_0 = 30°$, consider the effects of gaseous absorption with an absorption optical thickness $\tau_g = 0.1$ and 0.2, introduced separately at 0.75 and 2.16 μm, and droplet absorption at 2.16 μm with a refractive index $m = 1.294–0.0005i$.

introduction of gaseous absorption at 2.16 μm, on the other hand, leads to a systematic overestimation of the effective radius, relatively independent of effective radius. These simulations are in reasonable agreement with the results presented in Fig. 8, except in instances for which drizzle-sized droplets were present in significant concentrations and were largely undetected by our method. The introduction of additional absorption within the cloud droplets themselves (heavy solid line) results in an overestimation of the effective radius, with the overestimation tending to increase with increasing r_e. These results are inconsistent with our results and those of King et al. (1990), who found a close agreement between the single scattering albedo of the cloud layer at 2.16 μm obtained from theoretical calculations and experimental observations.

To further clarify the preceding discussion, we computed the difference between r_{center} and $r_{\text{in situ}}$ for all observations for which $6 \leqslant r_{\text{in situ}} \leqslant 7$ μm (cf. Fig. 8). These results, presented in Fig. 16a as a function of the remote sensing-derived cloud optical thickness, show that the overestimation of effective radius by our remote sensing technique tends to decrease as the optical thickness increases, Superimposed on these results are theoretical simulations of the effect of introducing gaseous absorption with an optical thickness $\tau_g(2.16\ \mu\text{m}) = 0.1$ (dot-dashed curve) and 0.2 (dotted curve). These simulated retrievals at $\tau_c = 20$ are the same results presented in Fig. 15b at $r_e = 6.5$ μm, and suggest how Fig. 15b would be modified as the cloud optical thickness varies. In general, our experimental observations presented in Fig. 16a are consistent with $\tau_g(2.16\ \mu\text{m}) \geqslant 0.2$.

Since the experimental observations presented in Fig. 16a were obtained in clouds of varying geometrical thicknesses, we have found it useful to transform the abscissa scale from optical thickness to scaled volume extinction coefficient, defined by

$$\beta'_{\text{ext}} = \frac{\beta_{\text{ext}}}{1 - 0.33\tau_c e^{-0.26\tau_c}} \tag{5}$$

where $\beta_{\text{ext}} = \tau_c/(z_t - z_b)$ is the volume extinction coefficient of the cloud layer. The denominator of this expression, a consequence of asymptotic theory, is required in order to make the two theoretical curves of Fig. 16a, which have different values of the gaseous absorption optical thickness but the same gaseous absorption coefficient $\beta_g(2.16\ \mu\text{m}) = 0.6\ \text{km}^{-1}$, virtually collapse into a single curve when transformed as in Fig. 16b. The experimental results presented in Fig. 16b show that by eliminating the geometrical thickness of the cloud layer the observed overestimation of effective radius decreases as β'_{ext} increases, and that this overestimation is more nearly a unique function of β'_{ext} than of τ_c (cf. Figs. 16a and 16b). In addition to these retrieval results, Fig. 16b shows simulations of the effect of gaseous absorption within the cloud layer for $\beta_g(2.16\ \mu\text{m}) = 0.3$, 0.6 and 0.9 km^{-1}. These simulations suggest that $\beta_g(2.16\ \mu\text{m})$ ranges between 0.5 and 0.7 km^{-1} for the clouds that we sampled during the FIRE IFO. If this enhanced absorption is due to water vapor, our gaseous absorption coefficient of 0.6 km^{-1} is equivalent to a mass absorption coefficient of 0.6 $\text{cm}^2\ \text{g}^{-1}$ at the cloud temperature of our observations (285 K).

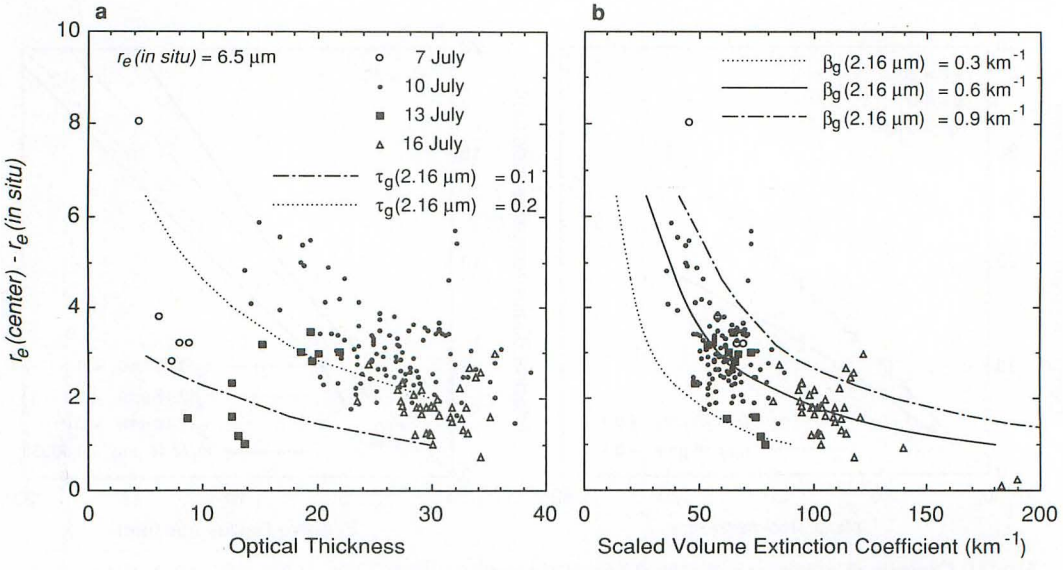

FIG. 16. Scatter plot of $r_{\text{center}} - r_{\text{in situ}}$ as a function of (a) τ_{remote} and (b) β'_{ext} for all observations presented in Fig. 8 for which $6 \leqslant r_{\text{in situ}} \leqslant 7$ μm. Superimposed on these results are corresponding differences between the effective radius derived from simulated remote sensing measurements in which gaseous absorption is introduced within the cloud layer at 2.16 μm.

Finally, we have performed simulations of the effect of enhanced water vapor absorption above the cloud layer on our retrieval of cloud optical thickness and effective radius. These computations show that 1) the bias in the retrieved value of the effective radius is largely independent of effective radius, as in Fig. 15b for the case of water vapor absorption within the cloud, and 2) this bias is approximately *independent* of β'_{ext}, in contrast to the results presented in Fig. 16b. If the column loading of water vapor above the cloud layer w_g ranges between 0.3 and 0.6 g cm^{-2}, the probable value of $\beta_g(2.16\ \mu\text{m})$ ranges between 0.15 and 0.25 km^{-1}, in contrast to 0.6 km^{-1} for the case of no water vapor absorption above the cloud layer.

9. Conclusions

High-resolution images of the spectral reflection function of clouds were obtained with the Multispectral Cloud Radiometer (MCR) operated from the NASA ER-2 aircraft during the intensive field observation component of the FIRE marine stratocumulus experiment, conducted off the coast of southern California between 29 June and 18 July 1987. Multispectral images of the reflection function at 0.75 and 2.16 μm were used to derive the optical thickness, effective particle radius and liquid water path of stratiform cloud layers on four days (7, 10, 13 and 16 July), where each image was approximately 35 km in width and ranged between 105 and 165 km in length, depending on day. In addition to these high-altitude aircraft measurements, Landsat-5 Thematic Mapper (TM) scenes were acquired and analyzed on two days (7 and 16 July).

One of the unique aspects of this experiment was the ability to coordinate remote sensing measurements with nearly simultaneous in situ microphysical measurements, in our case obtained with the University of Washington C-131A aircraft. This use of multiple aircraft provided us the unparalleled opportunity to compare the remote sensing-derived cloud optical thickness, effective radius and liquid water path with comparable in situ microphysical estimates obtained along the nadir track of the ER-2 aircraft, an opportunity unavailable to Twomey and Cocks (1982, 1989), Foot (1988) and Rawlins and Foot (1990), who made use of sequential remote sensing and in situ measurements obtained from a single aircraft.

Our comparisons between in situ and remote sensing-derived values of the effective radius (Figs. 3, 8 and 16) have demonstrated that remote sensing consistently overestimates the radius of cloud droplets, even after allowing for the effects of vertical inhomogeneity in the retrieval process. These findings are in close accord with the conclusions of Twomey and Cocks (1989) and Rawlins and Foot (1990), and further support the mounting evidence that clouds reflect less solar radiation at 2.16 μm than theory predicts. Furthermore, our results, obtained in four marine stratocumulus clouds having a wide range of microphysical conditions, reveal that the bias in the derived value of the effective radius is typically 2–3 μm, with a weak dependence on the magnitude of the effective radius and an overall tendency to decrease as the cloud optical thickness increases, in support of Stephens and Tsay's (1990) hypothesis that a previously unaccounted for water vapor continuum is present in the near-infrared. For large values of the effective radius remote sensing tends to underestimate the effective radius because of an inability to detect the presence of large drizzle-sized droplets typically found low in the cloud layer.

In contrast to these results, our remote sensing estimates of the cloud optical thickness are generally in close agreement with corresponding estimates obtained from in situ microphysical measurements, with differences typically $\leqslant 10$ (cf. Figs. 4 and 9a). In this case, however, the in situ microphysical estimates were based on liquid water content measurements obtained with the Johnson-Williams hot wire probe, in addition to in situ measurements of the effective radius and estimates of the geometrical thickness of the cloud layer, and as such are expected to be less reliable than the more direct remote sensing estimates. If anything, these comparisons reveal a slight tendency for remote sensing to overestimate the cloud optical thickness when the optical thickness is small and to underestimate it with the optical thickness is large.

Joint probability density functions of the cloud optical thickness (τ_c) and effective radius (r_e) have been constructed from our analyses of MCR images on four days during FIRE (Fig. 10a). Corresponding results for the liquid water path (W) and r_e are presented in Fig. 10b. These statistical properties of the stratocumulus clouds that we observed reveal a distinct positive correlation between τ_c (or W) and r_e on the optically thin days of 7 and 13 July, and a modest negative correlation on the optically thick, drizzle-dominated days of 10 and 16 July. These results are further supported by our examination of in situ microphysical measurements alone, presented in Fig. 11. Our remote sensing and in situ microphysical measurements generally reveal droplet radii larger than Stephens (1978) found in his study, which was based solely on in situ FSSP measurements.

Marginal probability density functions of τ_c, W and r_e have also been constructed from the joint probability density functions presented in Fig. 10. These results, presented in Figs. 12–14, show that the marginal probability density functions of marine stratocumulus clouds are typically monomodal. Furthermore, we have shown that the probability density function of τ_c can be fit to a log-normal function, with a mode optical thickness ranging from 10 to 28, depending on day (Table 3). The probability density function of τ_c on 10 July is bimodal, and arises from the presence of a

high concentration of drizzle droplets low in the cloud, droplets which we were only able to detect in those portions of the cloud for which the optical thickness was small.

In order to explain the observed discrepancy between in situ and remote sensing estimates of the effective radius, we have found it necessary to introduce additional absorption by water vapor at 2.16 μm, as recently suggested by Stephens and Tsay (1990). We have found that our overestimate of the effective radius generally decreases as the optical thickness and volume extinction coefficient increase (Fig. 16), and that this bias is largely insensitive to the magnitude of the effective radius (cf. Figs. 8 and 15). Furthermore, we have demonstrated that a gaseous absorption coefficient of 0.5 to 0.7 km^{-1} is required at 2.16 μm in order to bring remote sensing and in situ estimates of r_e into close accord if we assume the additional gaseous absorption is restricted to the cloud layer alone. On the other hand, if additional water vapor absorption is proportionally added both above and within the cloud layer, an absorption coefficient of 0.15 to 0.25 km^{-1} is sufficient to explain the bias in our retrievals of the effective radius, consistent with the values proposed by Stephens and Tsay. Our observations are inconsistent with anomalous absorption within the cloud droplets themselves, either in the visible or near-infrared wavelength regions. Finally, before our method can reliably be applied to global satellite observations such as those to be obtained from the Moderate Resolution Imaging Spectrometer-Nadir (MODIS-N), to be flown as a NASA facility instrument on the Earth Observing System (EOS) (Salomonson et al. 1989) in the late 1990s, we are forced to recommend that further laboratory measurement of the optical properties of water vapor and liquid water be conducted in the critical wavelength region between 1.6 and 2.2 μm.

Acknowledgments. The authors are grateful to R. F. Cahalan of Goddard Space Flight Center for providing the Landsat-5 TM data, to D. P. Wylie of the University of Wisconsin for providing the GOES-6 visible image on 10 July 1987, to J. H. Lyons of the University of Washington for analyzing the FSSP and OAP cloud physics data, and to G. T. Arnold and H. G. Meyer for aid in performing the computations and for assistance in data analysis. We would further like to acknowledge the coordinating role of the FIRE Science Team, especially D. S. McDougal, D. B. Stroup and B. A. Albrecht. The research reported in this article was supported by NASA's Climate Program and by the National Science Foundation under Grant ATM-8615344.

APPENDIX

Spectral Albedo of the Ocean Surface

The amount of reflection by the underlying ocean surface is important for determining the optical properties of optically thin clouds. Under cloudy sky conditions it is sufficient to approximate the ocean surface as smooth and flat, such that the ocean reflectivity can be determined as follows:

$$A_g = \int_0^1 I_{\text{in}}^0(\mu) r(\mu) \mu d\mu \Big/ \int_0^1 I_{\text{in}}^0(\mu) \mu d\mu, \quad \text{(A1)}$$

where $r(\mu)$ is the Fresnel reflectance and $I_{\text{in}}^0(\mu)$ the azimuthally averaged solar radiation incident on the ocean surface. The effect of ocean waves and of upwelling radiation from the ocean surface can be neglected for $\lambda \geq 0.7$ μm and for radiation of small incident zenith angles, directions from which most of the transmitted solar radiation arises under overcast conditions (Nakajima and Tanaka 1983). If we expand the functions appearing in the integrands of (A1) by Legendre series of the form:

$$r(\mu) = \frac{1}{2} \sum_{l=0}^{\infty} (2l + 1) r_l P_l(2\mu - 1), \quad \text{(A2)}$$

$$I_{\text{in}}^0(\mu) = \frac{1}{2} \sum_{l=0}^{\infty} (2l + 1) k_l P_l(2\mu - 1), \quad \text{(A3)}$$

it follows upon substitution back into (A1) that

$$A_g = \frac{1}{2(k_0 + k_1)} \sum_{l=0}^{\infty} [l k_{l-1} + (2l + 1) k_l + (l + 1) k_{l+1}] r_l. \quad \text{(A4)}$$

The following two cases are especially important:

TABLE A1. Estimate of the ocean surface reflectivity under cloudy sky conditions.

λ (μm)	r_0	r_1	r_2	k_0	k_1	Isotropic A_g	Asymptotic A_g	Measured* A_g
0.75	0.34635	−0.21385	0.10761	1.6972	0.30286	0.0663	0.0502	0.0607
1.65	0.34046	−0.21274	0.10788	1.4390	0.26160	0.0639	0.0477	0.0426
2.16	0.33104	−0.21072	0.10825	1.2791	0.24268	0.0602	0.0438	0.0404

* Adapted from King et al. (1990).

(a) Isotropic incidence ($I^0_{\text{in}}(\mu) = \text{const}$)

$$A_g = \frac{1}{2}(r_0 + r_1), \tag{A5}$$

(b) Asymptotic incidence ($I^0_{\text{in}}(\mu) \approx a + b\mu$)

$$A_g = \frac{(r_0 + r_1)k_0 + (r_0 + 3r_1 + 2r_2)k_1}{2(k_0 + k_1)}. \tag{A6}$$

Table A1 gives the values of A_g determined from these expressions at selected MCR wavelengths, where the coefficients r_l and k_l were derived from numerical integrations of the expressions for r_l and k_l that result when Eqs. (A2) and (A3) are convolved with the Legendre polynomials $P_l(2\mu - 1)$ and integrated over μ from 0 to 1. We have also included ocean surface albedos measured by the CAR (King et al. 1990) during the FIRE marine stratocumulus experiment, values which are seen to be in reasonable accord with (A6) under cloudy sky conditions.

REFERENCES

Ackerman, S. A., and S. K. Cox, 1981: Aircraft observations of the shortwave fractional absorptance of non-homogeneous clouds. *J. Appl. Meteor.*, **20,** 1510–1515.

Albrecht, B. A., 1989: Aerosols, cloud microphysics, and fractional cloudiness. *Science,* **245,** 1227–1230.

——, D. A. Randall and S. Nicholls, 1988: Observations of marine stratocumulus clouds during FIRE. *Bull. Amer. Meteor. Soc.,* **69,** 618–626.

Baumgardner, D., W. Strapp and J. E. Dye, 1985: Evaluation of the Forward Scattering Spectrometer Probe. Part II: Corrections for coincidence and dead-time losses. *J. Atmos. Oceanic Technol.,* **2,** 626–632.

Betts, A. K., and W. Ridgway, 1989: Climatic equilibrium of the atmospheric convective boundary layer over a tropical ocean. *J. Atmos. Sci.,* **46,** 2621–2641.

Brenguier, J. L., 1989: Coincidence and dead-time corrections for particle counters. Part II: High concentration measurements with an FSSP. *J. Atmos. Oceanic Technol.,* **6,** 585–598.

Cahalan, R. F., M. Nestler, W. Ridgway, W. J. Wiscombe and T. Bell, 1989: Marine stratocumulus spatial structure. *Proc. 4th International Meeting on Statistical Climatology,* Rotorua, New Zealand, 19–25.

Chýlek, P., K. Ya. Kondratyev and J. Hallett, 1989: Graphitic carbon and broadband absorption of solar radiation by clouds. *IRS '88: Current Problems in Atmospheric Radiation,* J. Lenoble and J. F. Geleyn, Eds., A. Deepak, 38–41.

Curran, R. J., H. L. Kyle, L. R. Blaine, J. Smith and T. D. Clem, 1981: Multichannel scanning radiometer for remote sensing cloud physical parameters. *Rev. Sci. Instrum.,* **52,** 1546–1555.

Downing, H.D., and D. Williams, 1975: Optical constants of water in the infrared. *J. Geophys. Res.,* **80,** 1656–1661.

Durkee, P. A., 1989: Observations of aerosol-cloud interactions in satellite-detected visible and near-infrared intensity. *Proc. Symposium on the Role of Clouds in Atmospheric Chemistry and Global Climate,* American Meteorological Society, Anaheim, CA, 157–160.

Foot, J. S., 1988: Some observations of the optical properties of clouds. I: Stratocumulus. *Quart. J. Roy. Meteor. Soc.,* **114,** 129–144.

Gorodetskiy, A. K., I. S. Kuznetsov, V. Ye. Lystsev and V. I. Syachinov, 1980: Light scattering coefficients in layered clouds. *Izv. Acad. Sci. USSR, Atmos. Ocean. Phys.,* **16,** 494–499.

Herman, G. F., and J. A. Curry, 1984: Observational and theoretical studies of solar radiation in arctic stratus clouds. *J. Climate Appl. Meteor.,* **23,** 5–24.

King, M. D., 1987: Determination of the scaled optical thickness of clouds from reflected solar radiation measurements. *J. Atmos. Sci.,* **44,** 1734–1751.

——, M. G. Strange, P. Leone and L. R. Blaine, 1986: Multiwavelength scanning radiometer for airborne measurements of scattered radiation within clouds. *J. Atmos. Oceanic Technol.,* **3,** 513–522.

——, L. F. Radke and P. V. Hobbs, 1990: Determination of the spectral absorption of solar radiaton by marine stratocumulus clouds from airborne measurements within clouds. *J. Atmos. Sci.,* **47,** 894–907.

King, W. D., 1984: Air flow and particle trajectories around aircraft fuselages. I: Theory. *J. Atmos. Oceanic Technol.,* **1,** 5–13.

——, D. A. Parkin and R. J. Handworth, 1978: A hot wire liquid water device having fully calculable response characteristics. *J. Appl. Meteor.,* **17,** 1809–1813.

Kloesel, K. A., B. A. Albrecht and D. P. Wylie, 1988: FIRE marine stratocumulus observations—Summary of operations and synoptic conditions. FIRE Tech. Rept. No. 1, Department of Meteorology, Pennsylvania State University, University Park, PA, 171 pp.

Kneizys, F. X., E. P. Shettle, W. O. Gallery, J. H. Chetwynd, L. W. Abreu, J. E. A. Selby, R. W. Fenn and R. A. McClatchey, 1980: Atmospheric transmittance/radiance: Computer code LOWTRAN 5. AFGL-TR-80-0067, Air Force Geophysics Laboratories, Hanscom AFB, 233 pp.

Knollenberg, R. G., 1981: Techniques for probing cloud microstructure. *Clouds: Their Formation, Optical Properties, and Effects,* P. V. Hobbs and A. Deepak, Eds., Academic Press, 15–91.

MacPherson, J. I., and D. Baumgardner, 1988: Air-flow about King Air wing-tip mounted cloud particle measurement probes. *J. Atmos. Oceanic Technol.,* **5,** 259–273.

Nakajima, T., and M. Tanaka, 1983: Effect of wind-generated waves on the transfer of solar radiation in the atmosphere-ocean system. *J. Quant. Spectrosc. Radiat. Transfer,* **29,** 521–537.

——, and M. D. King, 1990: Determination of the optical thickness and effective particle radius of clouds from reflected solar radiation measurements. Part I: Theory. *J. Atmos. Sci.,* **47,** 1878–1893.

Newiger, M., and K. Bähnke, 1981: Influence of cloud composition and cloud geometry on the absorption of solar radiation. *Contrib. Atmos. Phys.,* **54,** 370–382.

Noonkester, V. R., 1985: Profiles of optical extinction coefficients calculated from droplet spectra observed in marine stratus cloud layers. *J. Atmos. Sci.,* **42,** 1161–1171.

Palmer, K. F., and D. Williams, 1974: Optical properties of water in the near infrared. *J. Opt. Soc. Amer.,* **64,** 1107–1110.

Personne, P., J. L. Brenguier, J. P. Pinty and Y. Pointin, 1982: Comparative study and calibration of sensors for the measurement of the liquid water content of clouds with small droplets. *J. Appl. Meteor.,* **21,** 189–196.

Radke, L. F., J. A. Coakley, Jr. and M. D. King, 1989: Direct and remote sensing observations of the effects of ships on clouds. *Science,* **246,** 1146–1149.

Randall, D. A., J. A. Abeles and T. G. Corsetti, 1985: Seasonal simulations of the planetary boundary layer and boundary-layer stratocumulus clouds with a general circulation model. *J. Atmos. Sci.,* **42,** 641–676.

Rawlins, F., and J. S. Foot, 1990: Remotely sensed measurements of stratocumulus properties during FIRE using the C130 aircraft multichannel radiometer. *J. Atmos. Sci.,* **47,** 2488–2503.

Salomonson, V. V., W. L. Barnes, P. W. Maymon, H. E. Montgomery and H. Ostrow, 1989: MODIS: Advanced facility instrument for studies of the Earth as a system. *IEEE Trans. Geosci. Remote Sens.,* **27,** 145–153.

Schiffer, R. A., and W. B. Rossow, 1983: The International Satellite Cloud Climatology Project (ISCCP): The first project of the World Climate Research Programme. *Bull. Amer. Meteor. Soc.*, **64,** 779–784.

Slingo, A., 1989: A GCM parameterization for the shortwave radiative properties of water clouds. *J. Atmos. Sci.*, **46,** 1419–1427.

——, S. Nicholls and J. Schmetz, 1982: Aircraft observations of marine stratocumulus during JASIN. *Quart. J. Roy. Meteor. Soc.*, **108,** 833–856.

Spinhirne, J. D., R. Boers and W. D. Hart, 1989: Cloud top liquid water from lidar observations of marine stratocumulus. *J. Appl. Meteor.*, **28,** 81–90.

Stephens, G. L., 1978: Radiation profiles in extended water clouds. II: Parameterization schemes. *J. Atmos. Sci.*, **35,** 2123–2132.

——, and C. M. R. Platt, 1987: Aircraft observations of the radiative and microphysical properties of stratocumulus and cumulus cloud fields. *J. Climate Appl. Meteor.*, **26,** 1243–1269.

——, and S. C. Tsay, 1990: On the cloud absorption anomaly. *Quart. J. Roy. Meteor. Soc.*, **116,** 671–704.

Twohy, C. H., A. D. Clarke, S. G. Warren, L. F. Radke and R. J. Charlson, 1989: Light-absorbing material extracted from cloud droplets and its effect on cloud albedo. *J. Geophys. Res.*, **94,** 8623–8631.

Twomey, S., 1972: The effect of cloud scattering on the absorption of solar radiation by atmospheric dust. *J. Atmos. Sci.*, **29,** 1156–1159.

——, 1977: The influence of pollution on the shortwave albedo of clouds. *J. Atmos. Sci.*, **34,** 1149–1152.

——, and T. Cocks, 1982: Spectral reflectance of clouds in the near-infrared: Comparison of measurements and calculations. *J. Meteor. Soc. Japan,* **60,** 583–592.

——, and ——, 1989: Remote sensing of cloud parameters from spectral reflectance in the near-infrared. *Beitr. Phys. Atmos.*, **62,** 172–179.

Welch, R. M., S. K. Cox and J. M. Davis, 1980: *Solar Radiation and Clouds.* Meteor. Monogr. No. 39, Amer. Meteor. Soc., 96 pp.

Wielicki, B. A., and L. Parker, 1989: Cloud properties observed using Landsat satellite data. *IRS '88: Current Problems in Atmospheric Radiation,* J. Lenoble and J. F. Geleyn, Eds., A. Deepak, 161–164.

Wiscombe, W. J., R. M. Welch and W. D. Hall, 1984: The effects of very large drops on cloud absorption. Part I: Parcel models. *J. Atmos. Sci.*, **41,** 1336–1355.